Research Square

Preprints are preliminary reports that have not undergone peer review.
They should not be considered conclusive, used to inform clinical practice,
or referenced by the media as validated information.

Genomic and ecological specialization of Methanobrevibacter species shape human methane emission and overall gut ecosystem function

Christine Moissl-Eichinger

christine.moissl-eichinger@medunigraz.at

Medical University of Graz https://orcid.org/0000-0001-6755-6263

Christina Kumpitsch

Medical University of Graz https://orcid.org/0000-0002-2077-2839

Alexander Mahnert

Medical University of Graz https://orcid.org/0000-0001-7083-8894

Stefanie Duller

Medical University of Graz

Marcus Blohs

Medical University of Graz

Rokhsareh Mohammadzadeh

Medical University of Graz

Laura Schmidberger

Medical University of Graz

Simone Vrbancic

Medical University of Graz

Tobias Madl

Medical University of Graz https://orcid.org/0000-0002-9725-5231

Hansjörg Habisch

Medical University of Graz https://orcid.org/0000-0001-5537-506X

Katharina Leithner

Medical University of Graz https://orcid.org/0000-0002-8252-9279

Theresa Haitzmann

Medical University of Graz

Sonja Lackner

Medical University of Graz

Sandra Holasek

Medical University of Graz

Christoph Högenauer
Department of Internal Medicine, Medical University of Graz, A-8036 Graz https://orcid.org/0000-0003-4566-0806
Adrian Moser
Medical University of Graz
Tamara Zurabischvili
Medical University of Graz
Christian Diener
Medical University of Graz https://orcid.org/0000-0002-7476-0868

Article

Keywords:

Posted Date: November 2nd, 2026

DOI: https://doi.org/10.21203/rs.3.rs-11389263/v1

License: This work is licensed under a Creative Commons Attribution 4.0 International License.
Read Full License

Additional Declarations: There is **NO** Competing Interest.

Genomic and ecological specialization of *Methanobrevibacter* species shape human methane emission and overall gut ecosystem function

Christina Kumpitsch[1,2], Alexander Mahnert[1,2], Stefanie Wimberger[1], Marcus Blohs[1], Rokhsareh Mohammadzadeh[1], Laura Schmidberger[1], Simone Vrbancic[1], Tobias Madl[2,3], Hansjörg Habisch[3], Katharina Leithner[2,4,5], Theresa Haitzmann[4], Sonja Lackner[6], Sandra Holasek[6], Christoph Högenauer[2,7], Adrian Mathias Moser, Tamara Zurabischvili[1], Christian Diener[1], Christine Moissl-Eichinger[1,2]

Corresponding author: Christine Moissl-Eichinger; christine.moissl-eichinger@medunigraz.at

[1] Diagnostics and Research Institute of Hygiene, Microbiology and Environmental Medicine, Medical University of Graz, Graz, Austria
[2] BioTechMed Graz, Graz, Austria
[3] Division Medicinal Chemistry, Otto Loewi Research Center, Medical University of Graz, Graz, Austria
[4] Division of Pharmacology, Otto Loewi Research Center, Medical University of Graz, Graz, Austria
[5] Lung Research Cluster, Medical University of Graz, Graz, Austria
[6] Division of Pathophysiology and Immunology, Otto Loewi Research Center, Medical University of Graz, Graz, Austria
[7] Division of Gastroenterology and Hepatology, Department of Internal Medicine, Medical University of Graz, Graz, Austria

Abstract

Methane is a unique archaeal metabolite that links gut microbial ecology to host physiology. Although intestinal methane production varies by several orders of magnitude between individuals and has been associated with gastrointestinal transit and disease states, the ecological and functional determinants underlying this variation remain poorly understood.

Here, we integrate breath methane phenotyping with shotgun metagenomics, metatranscriptomics, comparative genomics, cultivation and stable-isotope tracing in 80 deeply characterized individuals to determine the species-level and functional basis of human gut methanogenesis.

Breath methane levels strongly reflected archaeal abundance but could not fully explain methane emission; species-resolved profiling revealed that methane emission represents distinct archaeome states rather than differences in methanogen quantity alone. High methane emitters were dominated by *Methanobrevibacter smithii* and *M. intestini*, whereas low emitters harbored a previously uncharacterized *Methanobrevibacter* lineage (*M.* sp900766745), for which we propose the name *Candidatus* Methanobrevibacter hominipaucus sp. nov.

Comparative genomics revealed that *M.* sp900766745 represents a metabolically streamlined lineage lacking several methyl-compound utilization pathways and displaying reduced substrate acquisition capacity. Communities of low-emission individuals exhibited reduced microbial transcriptional activity and accumulated incompletely processed dietary metabolites, indicating lower fermentative turnover and altered hydrogen flux.

Introduction

Methane is the major gaseous end product of human gut microbial metabolism that can be quantified non-invasively in exhaled breath, providing a direct readout of microbial metabolism. Unlike most microbial metabolites, methane is produced exclusively by methanogenic archaea, which colonize more than 90% of adults but typically comprise only ~1% of the gut microbiome [1–3]. Breath methane production varies by several orders of magnitude between individuals, with methanogens accounting for approximately 2% of the gut microbiome in high methane emitters but as little as 0.002% in low emitters [4]. This variation follows striking demographic patterns. The prevalence of high methane producers ranges from approximately 14% in East Asian populations to nearly 80% in populations of African ancestry, whereas European and Middle- to West-Asian populations typically exhibit intermediate frequencies of 24-60% (mean ~44%) [reviewed in [5]. Methane production increases with age and has been associated with positive and negative health outcomes, including constipation-predominant irritable bowel syndrome, intestinal methanogen overgrowth (IMO), colorectal cancer, slower intestinal transit, altered intestinal pH and a lean host phenotype [3,6–12]. The reason for this striking inter-individual variation in methane production, however, remains poorly understood.

Methanogens occupy a distinctive ecological niche in the gut as terminal consumers of hydrogen generated during bacterial fermentation. By converting hydrogen, carbon dioxide and methylated compounds to methane, methanogens maintain low hydrogen partial pressures that can thermodynamically favor continued bacterial fermentation and thereby influence microbial carbon and energy flux despite their low abundance [13–16].

Analyzing the role of archaea is challenging, as they remain systematically underrepresented in microbiome research. Archaea represent a distinct domain of life, and thereby differ substantially from bacteria in terms of their genetic makeup and metabolic pathways [17,18]. 16S rRNA gene sequencing approaches incompletely recover archaeal diversity, and much of our current understanding of human methanogens derives from cultivation or targeted qPCR studies performed in relatively small cohorts [18,19]. Consequently, gut methanogenesis has largely been viewed through the lens of a single dominant species, *Methanobrevibacter smithii* (very recently reclassified as *Methanocatella smithii* [20]), which has long been considered the principal methanogen of the human intestine [4,21,22]. Recent genome-resolved metagenomic studies, however, have revealed previously unrecognized diversity within human-associated *Methanobrevibacter*, including *M. intestini* (recently reclassified as *Methanocatella intestini* [20])[1,23] and an uncultivated species-level lineage provisionally designated *Methanobrevibacter* sp900766745 [24].

These discoveries raise a fundamental ecological question: does variation in human methane production primarily reflect the abundance of methanogens, or does it arise from differences in the ecological strategies and metabolic capabilities of individual methanogen species? In particular, differences in substrate utilization, hydrogen consumption and energy conservation could alter how individual methanogen lineages interact with bacterial fermenters, while host factors such as gastrointestinal transit may further shape substrate availability, hydrogen gradients and the physicochemical environment in which these interactions occur.

Here, we resolve the species-level and functional determinants of human methane production by integrating breath methane phenotyping with shotgun metagenomics, metatranscriptomics, cultivation, comparative genomics, metabolomics, and stable-isotope tracing in 80 deeply characterized individuals. We identify three recurrent *Methanobrevibacter*-dominated archaeome states associated with distinct methane emission phenotypes and show that these states differ not only in methanogen abundance but also in species composition, genomic potential, hydrogen metabolism, bacterial community structure, and microbial activity. We further characterize a previously uncultivated, genomically streamlined lineage enriched in low methane emitters, for which we propose the name *Candidatus Methanobrevibacter hominipaucus* sp. nov., and identify lineage-specific differences in hydrogen utilization and substrate acquisition. Integrating these observations with metabolomic and isotope-tracing data reveals distinct patterns of downstream anaerobic carbon turnover and fermentation associated with the methanogen states. Together, our findings establish methane emission as a readout of alternative gut ecosystem configurations and reveal previously unrecognized ecological and metabolic specialization within the archaeal component of the human microbiome.

Results

Methane phenotype is a major determinant of gut microbiome variation

To determine whether methane production represents a determinant of gut microbiome variation, we analyzed a standardized cohort of 80 participants, with matched breath and stool samples collected using a harmonized recruitment, sampling and bioinformatic workflows optimized for archaeal detection. Participants were characterized for demographic variables (e.g., age, sex, BMI), gastrointestinal symptoms and habitual dietary intake (e.g., carbohydrate and protein intake). Breath methane concentrations were measured in the morning prior to food intake or oral hygiene procedures (**Supp. Tab. 01**). Individuals were classified by $CH4\ phenotypes$ into $high\ methane\ emitters\ (HE)$ or $low\ methane\ emitters\ (LE)$ using an established cut-off of 4 ppm [4]; they were further classified by their $health\ status$ ($healthy$ vs. $diseased$ (any GIT complaints) (**Fig. 1a** and **b**). Recruitment was balanced to obtain equally-sized groups of HE vs. LE (**Supp. Tab. 01**).

None of the recorded demographic variables (including age, sex, BMI) differed significantly between healthy and diseased participants, either across the full cohort or within the $CH4\ phenotypes$ subgroups. Across all participants, however, breath $methane\ emission\ [ppm]$ increased significantly with age (*spearman correlation (Sc)*, $p = 0.001$), and was negatively associated with $stool\ frequency$ ($p = 0.035$), consistent with previous associations between methane production, slower intestinal transit and constipation (**Table 1**) [8,11,18]. Archaeal abundance showed similar associations: the relative abundance of archaea (clr transformed) increased significantly with age ($p = 0.005$; Sc) and was inversely associated with $stool\ consistency$ ($p = 0.019$; Sc). The latter effect was accompanied by a decreased $stool\ frequency$ ($p = 0.041, Sc$) (**Table 1**).

We next asked whether methane phenotype or disease status better explained variation in the gut microbiome. Shotgun metagenomic profiling of stool samples (n = 66) revealed no significant differences in alpha or beta diversity or differential microbial abundance between healthy and diseased participants, likely reflecting the heterogeneity of the gastrointestinal conditions included in the study. In contrast, $CH4\ phenotypes$ (HE vs. LE) were associated with pronounced differences in microbial community structure (R^2 = 0.06; **Table 1**; **Fig. 1c**), indicating that methane formation constitutes a stronger determinant of microbiome organization than disease status in this cohort.

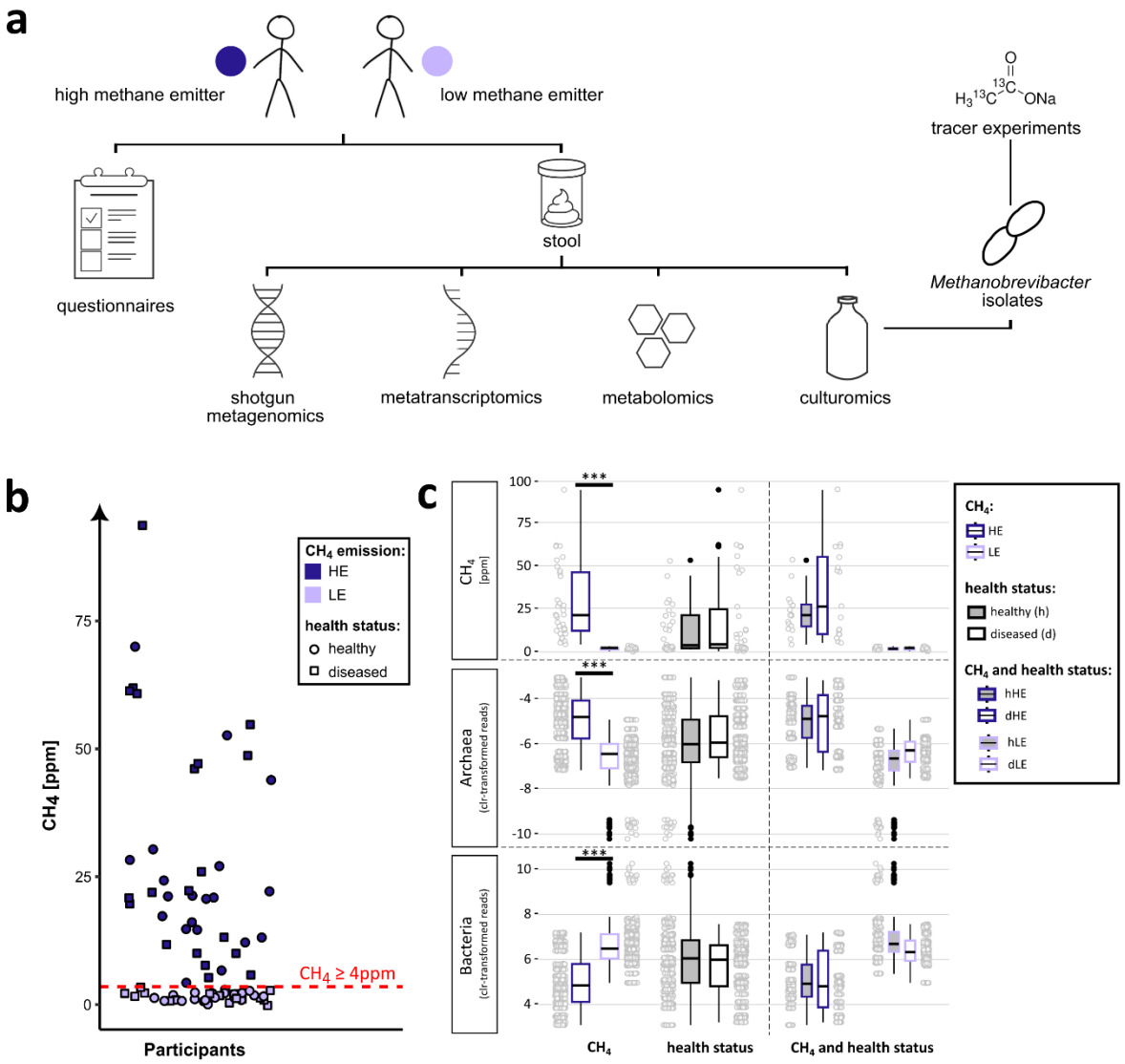


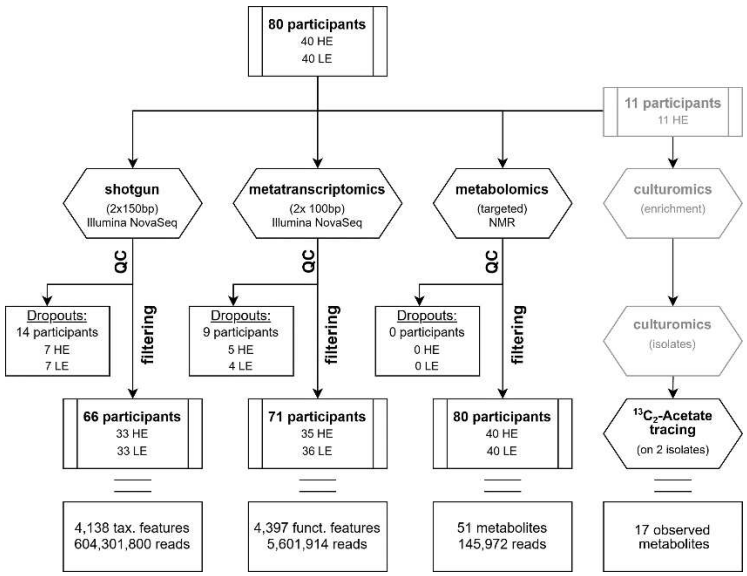
Figure 1. Overview of the dataset used in this study. a. Study design and methods used in this study. Questionnaires included general (e.g., age, sex, BMI), dietary (food frequency) and health-related (bowel movement and GIT health) information. Isolates of *M. smithii* and *M. intestini* were used to perform isotope tracing. (created using BioRender) **b.** Measured breath methane levels of all participants. The cut-off was set to 4 ppm for high methane emitters (CH_4 < 4 ppm - low methane emitters). **c.** Statistics of CH_4 levels and microbial reads based on metadata information health status, CH_4 emission, or combined (CH_4 emission and health status). archaeal and bacterial data were clr-transformed; HE - high methane emitter, LE - low methane emitter

Table 1. ***Statistics of general and microbial parameters of the participants based on methane emission phenotype (HE and LE) as well as health status (healthy and diseased).***

Sample Metadata Table

	in general				HE					LE				in general		
	all	healthy	diseased	*p*	HE	LE	*p*	healthy	diseased	*p*	healthy	diseased	*p*	Archaea		*p*
General parameters														*test*	T / corr. coef.	
participants, *n*	80	40	40	.	40	40	.	20	20	.	20	20	.	.	.	.
age, *median*	30	30	30	*0.435*	37.5	28.0	***0.0001***	35.5	39.5	*0.126*	29.0	28.0	*0.607*	*Spearman*	0.345	***0.005***
sex, *n* (female)	47	22	25	*0.496*	27	20	*0.112*	12	15	*0.112*	10	10	*1*	*t-test*	-2.138	***0.018***
BMI, *median*	22.1	22.4	22.1	*0.842*	22.4	21.9	*0.121*	22.5	22.3	*0.855*	22.0	21.2	*0.687*	*Spearman*	0.019	*0.881*
CH_4, *median* [ppm]	3.5	3.5	4	*0.812*	21.0	2.0	***7.99E-15***	21.0	22.0	*0.569*	1.5	2.0	*0.925*	*Spearman*	0.661	***1.58E-09***
smoker, *n* (yes)	7	3	4	*0.549*	6	1	*0.079*	3	3	*0.079*	0	1	*0.311*	*t-test*	0.324	*0.747*
birth mode, *n* (natural)	63	35	28	*0.119*	30	33	*0.189*	17	13	*0.189*	18	15	*0.376*	*t-test*	0.779	*0.427*
breastfed, *n* (yes)	70	38	34	*0.181*	34	38	*0.181*	18	16	*0.181*	20	0	*0.147*	*t-test*	-1.111	*0.271*
vegetarian, *n* (yes)	24	11	14	*0.450*	16	9	*0.291*	7	9	*0.240*	4	5	*0.283*	*t-test*	-0.677	*0.501*
stool frequency (per week)	6.75	6.5	7	*0.833*	6.0	7.0	***0.024***	6.0	7.0	*0.545*	7.5	7.0	*0.569*	*Spearman*	-0.256	***0.041***
stool consistency, *median*	3.4	3.0	3.5	*0.110*	3.0	3.5	*0.533*	3.0	3.0	*?*	3.0	4.0	*?*	*Spearman*	-0.288	***0.019***
IBS (yes)	13	0	13	***3.93E-15***	6	7	*0.950*	0	6	***0.028***	0	7	***0.014***	*t-test*	-0.189	*0.851*
Microbiome parameters																
participants, *n*	66	32	34	.	33	33	.	16	17	.	16	17	.	.	.	.
alpha diversity																
shannon, *median*	4.469	4.485	4.458	*0.990*	4.773	4.120	***9.39E-06***	4.833	4.680	*0.471*	4.087	4.167	*0.195*	.	.	.
richness, *median*	2014	2056	1975.5	*0.700*	2206	1822	***3.55E-06***	2250.5	2189	*0.207*	1799.5	1826	*0.296*	.	.	.
evenness, *median*	0.586	0.586	0.585	*0.857*	0.619	0.554	***2.13E-05***	0.626	0.607	*0.589*	0.543	0.556	*0.183*	.	.	.
beta diversity		R^2 = 0.7741		*0.890*	R^2 = 0.05597		***0.001***	R^2 = 0.9981		*0.450*	R^2 = 0.8447		*0.763*	.	.	.
microbial differences (at species level)		no significant			**569 significant**			no significant			no significant			.	.	.

…alpha diversity (Mann-Whitney U test)
…beta diversity (adonis2)
…microbial difference (ALDEx2; q-values)
…numerical (Mann-Whitney U test)
…nominal (Chi Square test)



Supplementary Figure X1. ***A schematic representation of the study design, showing all dropouts, filtered samples, and the features and reads obtained using each method.*** The grey-highlighted parts were performed in Ref [25]. HE - high methane emitters, LE - low methane emitters; QC - quality control

Methane emission is associated with methanogen abundance and distinct species-level Methanobrevibacter composition

We next determined whether differences in methane emission reflected variation in methanogen abundance. Shotgun metagenomic profiling revealed a strong positive association between breath methane concentrations [ppm] and archaeal read counts ($p = 3.01\ x\ 10^{-6}$*, linear regression model*, **Fig. 2a**). Consistently, HEs exhibited significantly higher archaeal signatures compared to LE ($q\ = 1.43\ x10^{-6}$, ALDEx2*;* **Fig. 2b**). However, archaeal abundance alone did not fully explain methane emission phenotype: archaeal loads varied substantially among HEs, while several LEs carried unexpectedly high archaeal abundances despite producing little CH_4 (**Fig. 2c**). Thus, methane emission is not determined by abundance alone.

The archaeal community was dominated by *Methanobrevibacter* (GTDB taxonomy: *Methanobrevibacter_A*), accounting for approx. 90% of archaeal reads in both groups (89.7% in HE, 90.25% in LE), with significantly higher abundance in HE ($q = 0.004$, ALDEx2) (**Figure 2d**). Species-level resolution revealed phenotypic-specific partitioning within this dominant genus: *M. smithii* (GTDB taxonomy: *Methanobrevibacter_A smithii*) and/or *M. intestini* (GTDB taxonomy: *Methanobrevibacter_A intestini*) were significantly enriched in HEs ($q = 5.76\ x\ 10^{-6}$ and $q = 1.25\ x\ 10^{-5}$, respectively, ALDEx2), while the uncultivated lineage *M.* sp900766745 was significantly enriched in LEs ($q = 0.018$, ALDEx2) (**Fig. 2d** and **2e; Supp. Tab. 02**).

Other archaeal genera, including *Methanosphaera* and *Methanomassiliicoccus*, were detected at substantially lower abundance. Among these, only *Methanomassiliicoccus* showed a modest enrichment in LEs ($q = 0.02$, ALDEx2) (**Supp. Fig. X2**; **Supp. Tab. 02**). No other archaeal signatures differed significantly between $CH4\ phenotypes$ or by $health\ status$ (**Supp. Tab. 02; Supp. Fig. X3**).

Breath methane concentration was positively correlated with all three *Methanobrevibacter* species, although the association did not reach significance for *M.* sp900766745 (*M. smithii*: $p = 0.00015$; *M. intestini*: $p = 0.043$; *M.* sp900766745: $p = 0.2422$, *linear regression*).

These findings indicate that methane emission reflects both the abundance and identity of dominant methanogens. We therefore focused subsequently on *M. smithii*, *M. intestini* and *M.* sp900766745 to resolve their species-specific ecological and functional characteristics.

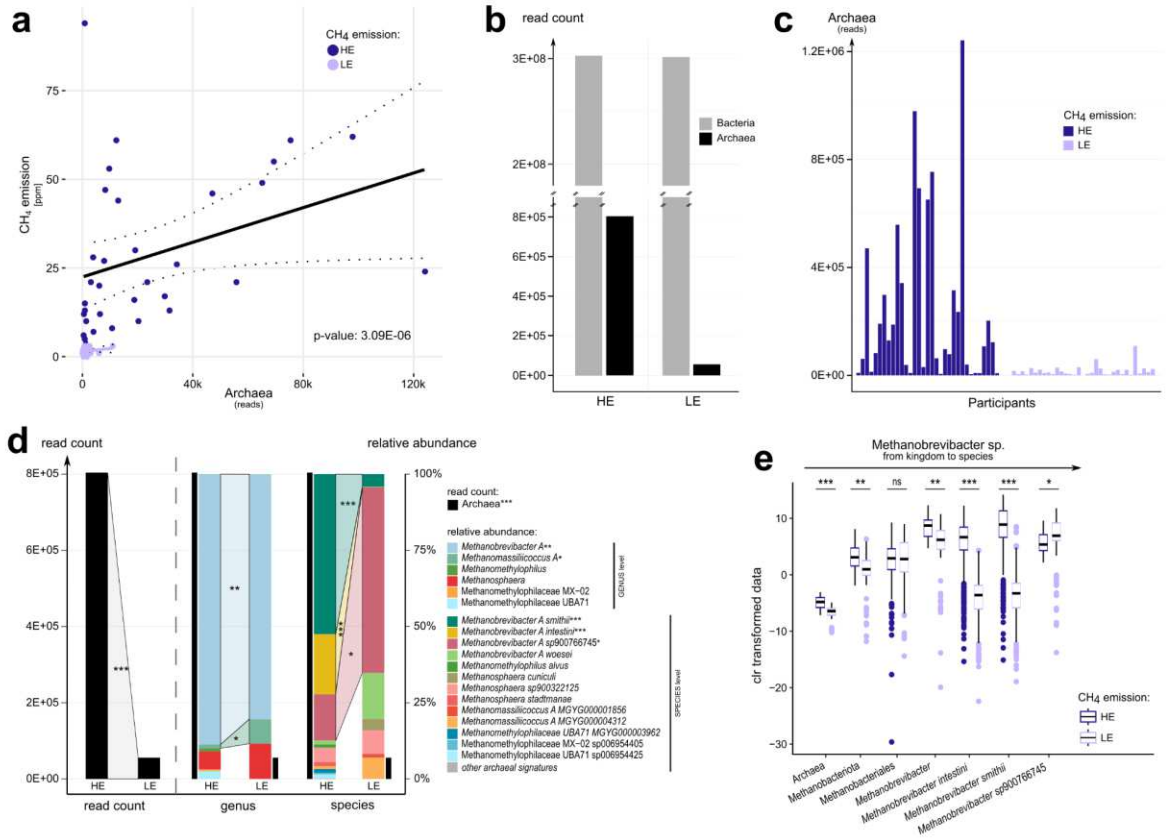
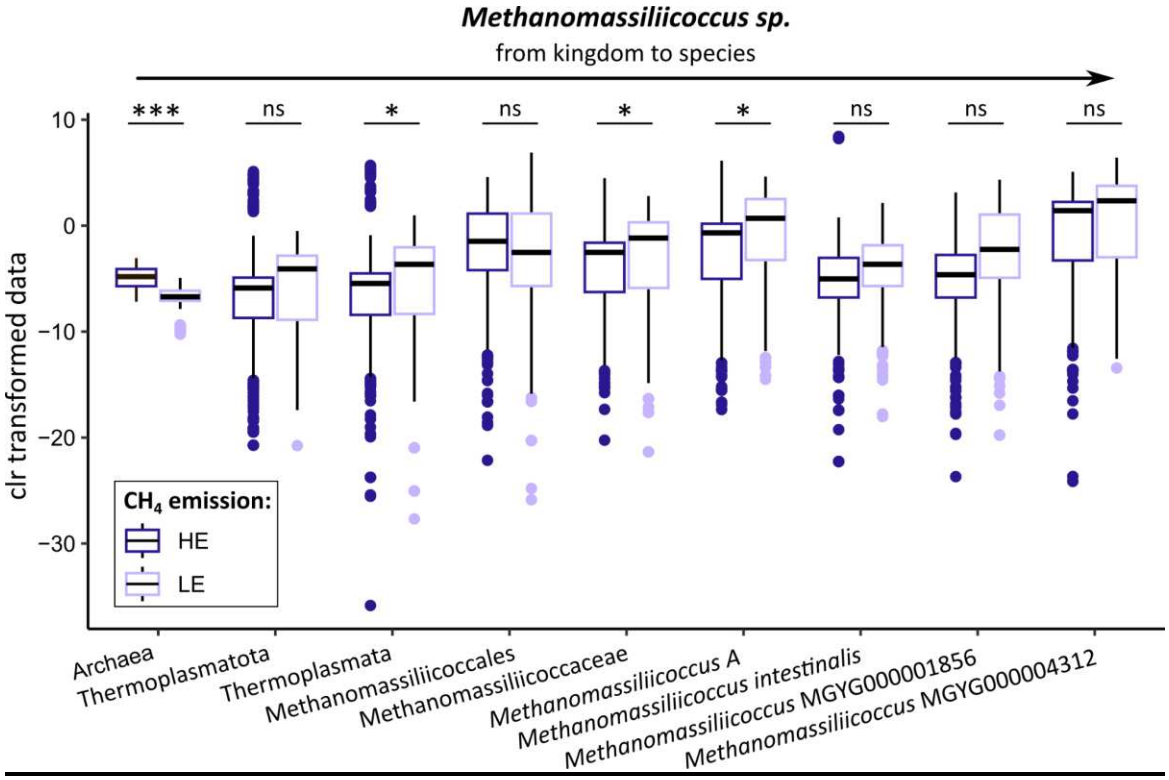
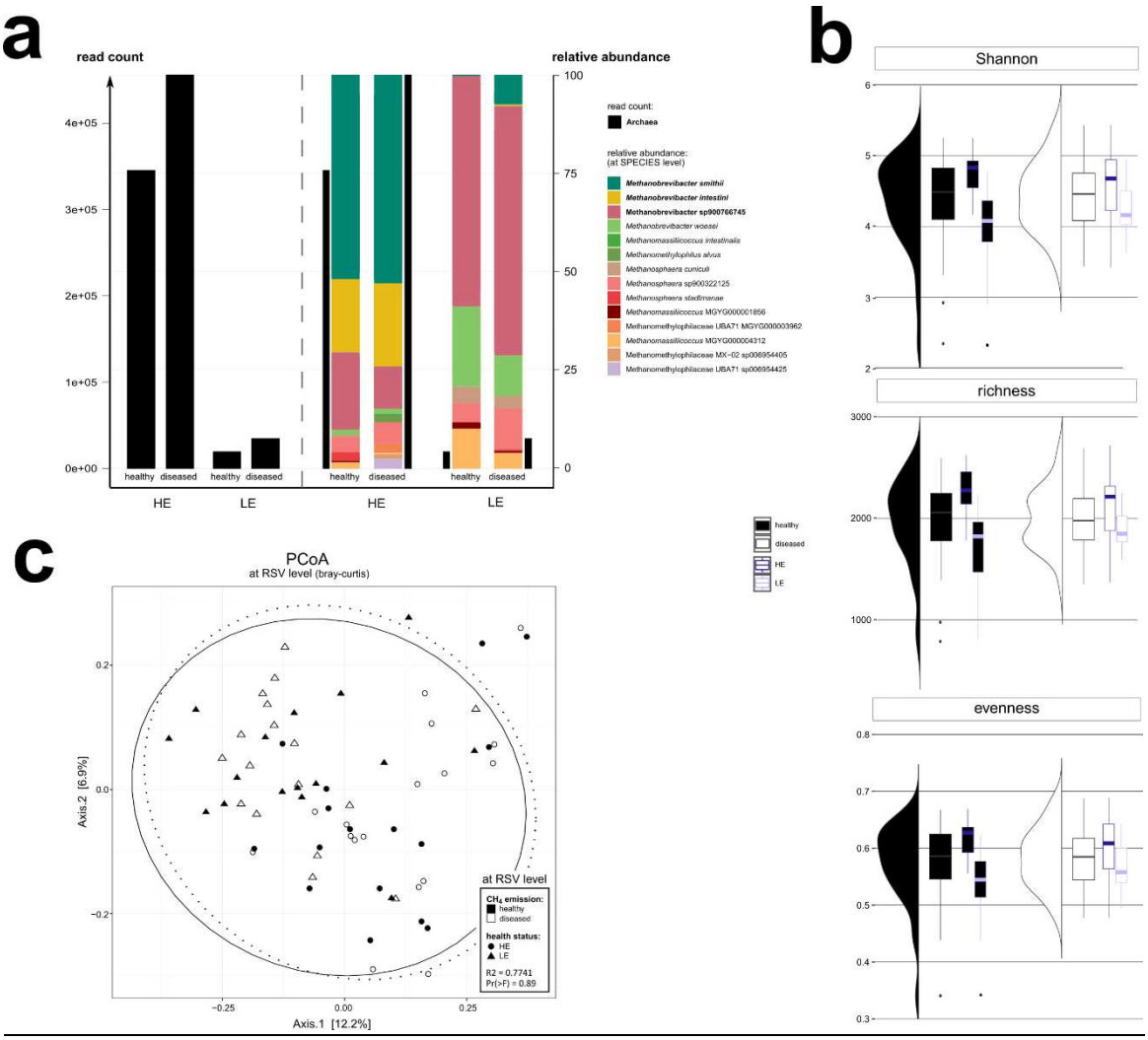


Figure 2. Archaeal signatures, especially of *Methanobrevibacter* species, are linked to methane emission. **a.** Significant positive correlation between CH_4 emission [ppm] and archaeal read counts (linear regression model) **b.** Bacterial and archaeal read counts in HE and LE samples. **c.** Higher archaeal read counts in nearly all high emitters compared to low emitting participants. **d.** Archaeal genera and species in HE and LE, respectively, show differences in *Methanobrevibacter* relative abundance. **e.** Differential abundance analysis of representatives of the *Methanobrevibacter* lineage (ALDEx2 - Archaea (*q=1.43e-06*); Methanobacteriota (*q=0.002*); Methanobacteria (*q=0.007*); Methanobacteriales (*q=0.961*); Methanobacteriaceae (*q=0.002*); *Methanobrevibacter A* (*q=0.004*); *Methanobrevibacter A smithii* (*q=5.76e-06*)/ *Methanobrevibacter A smithii A* (*q=1.25e-05*)/ *Methanobrevibacter A* sp900766745 (*q=0.018*)). Statistics based on clr-transformed data.



234

235 **Supp. Figure X2. Differential abundance of Methanomassiliicoccus sp. from kingdom to species based on**
236 **CH_4 emission phenotype.** ALDEx2: Archaea (*q*=1.43e-069); Thermoplasmatota (*q*=0.068); Thermoplasmata
237 (*q*=0.043); Methanomassiliicoccales (*q*=0.98); Methanomassiliicoccaceae (*q*=0.021); *Methanomassiliicoccus A*
238 (*q*=0.021); Methanomassiliicoccus intestinalis (*q*=0.442); Methanomassiliioccus MGYG000001856 (*q*=0.113);
239 Methanomassiliicoccus MGYG000004312 (*q*=0.075)



240

241 **Supp. Figure X3. Microbiome of HE and LE participants did not differ based on health status. a.** Read
242 counts and relative abundance of archaeal taxa in HE and LE based on methane and health groups. **b.** Alpha
243 diversity based on overall health status (black and white) as well as additionally separated by CH_4 phenotypes
244 (light and dark purple). **c.** Beta diversity based on the participants health status. HE - high methane emitter, LE -
245 low methane emitter.

Three Methanobrevibacter-dominated archaeome states define methane production in humans

Having established that $CH4\ phenotypes$ are associated with distinct *Methanobrevibacter* species, we ask whether gut archaeal communities create specific configurations rather than random combinations of methanogen species (**Fig. 3a**). Across the cohort, archaeal communities resolved into three predominant *Methanobrevibacter*-dominated states (**Fig. 3a**). HE individuals were predominantly characterized by *M. smithii* or *M. intestini*, whereas most LEs were dominated by the uncultivated lineage *M.* sp900766745. *M. smithii* accounted for >45% of archaeal reads in 22/33 HE samples, and *M. intestini* dominated in a further 7/33 samples; the remaining four HE samples were dominated by *M.* sp900766745 (**Fig. 3a, Supp. Fig. X4**). These individuals exhibited the lowest archaea-to-bacteria (A/B) ratios across the HE cohort with an archaeal relative abundance of less than 10 % (**Fig. 3a, Supp. Fig. X4**; **Supp. Fig. X5**) (median HE A/B = 0.0013; median LE A/B = 0.00013; based on read counts). Although *M. smithii* and *M. intestini* showed a weak positive association, their co-occurrence was not significant ($R2 = 0.0039$; $p = 0.62$; Sc), suggesting that they may occupy partially overlapping but distinct ecological niches rather than exhibiting strong competitive exclusion.

In contrast to HE individuals, most LEs were dominated by *M. sp900766745*, with only isolated exceptions exhibiting predominance of *M. smithii* or alternative archaeal taxa. The A/B ratio remained consistently lower in LEs compared to the HE median (**Fig. 3a, Supp. Fig. X5**).

Based on these recurrent abundance patterns, we classified archaeomes into three dominant *Methanobrevibacter* states: *M. smithii* (Ms), *M. intestini* (Mi) and *M.* sp900766745 (Msp). Ms- and Mi-archaeomes displayed higher archaeal richness compared with Msp-dominated communities (**Fig. 3b** and **3c**). Furthermore, individuals carrying Ms or Mi states represented the highest methane emitters, whereas Msp microbiome states and samples with negligible amounts of archaea ("No"; archaeal reads ≤10% of the overall microbiome) remained usually below the set high methane emission threshold (Ms and Mi compared to Msp and No ($p_{MsvsMsp}$= *5.0E-06;* $p_{MivsMsp}$= *9.0E-05;* p_{MsvsNo}= *1.5E-04;* p_{MivsNo}= *0.001*) (**Fig. 3d**).

The three states also differed in their associations with host phenotypes and hydrogen availability. The relative abundances of both *M. smithii* and *M. intestini* increased with age ($p = 0.002$ and $p = 0.001$, respectively) and were associated with markers of constipation, including lower stool frequency ($p = 0.004$ and $p = 0.003$) and constipation status ($p = 0.003$, and $p = 0.005$) (**Fig. 3e**). *M. intestini* abundance was negatively associated with breath hydrogen ($R2 = -.285$; $p = 0.021$), whereas *M.* sp900766745 showed the opposite

association ($R2 = 0.297$; $p = 0.016$), indicating differences in microbial hydrogen turnover, potentially reflecting increased production or decreased consumption in the different states. Among the remaining metadata variables, only female sex was associated with a significantly higher relative abundance of *M. smithii* (**Fig. 3e** and **3f**).

Our observations identify three recurrent *Methanobrevibacter* states that differ in methanogen composition, methane output and host-associated features.

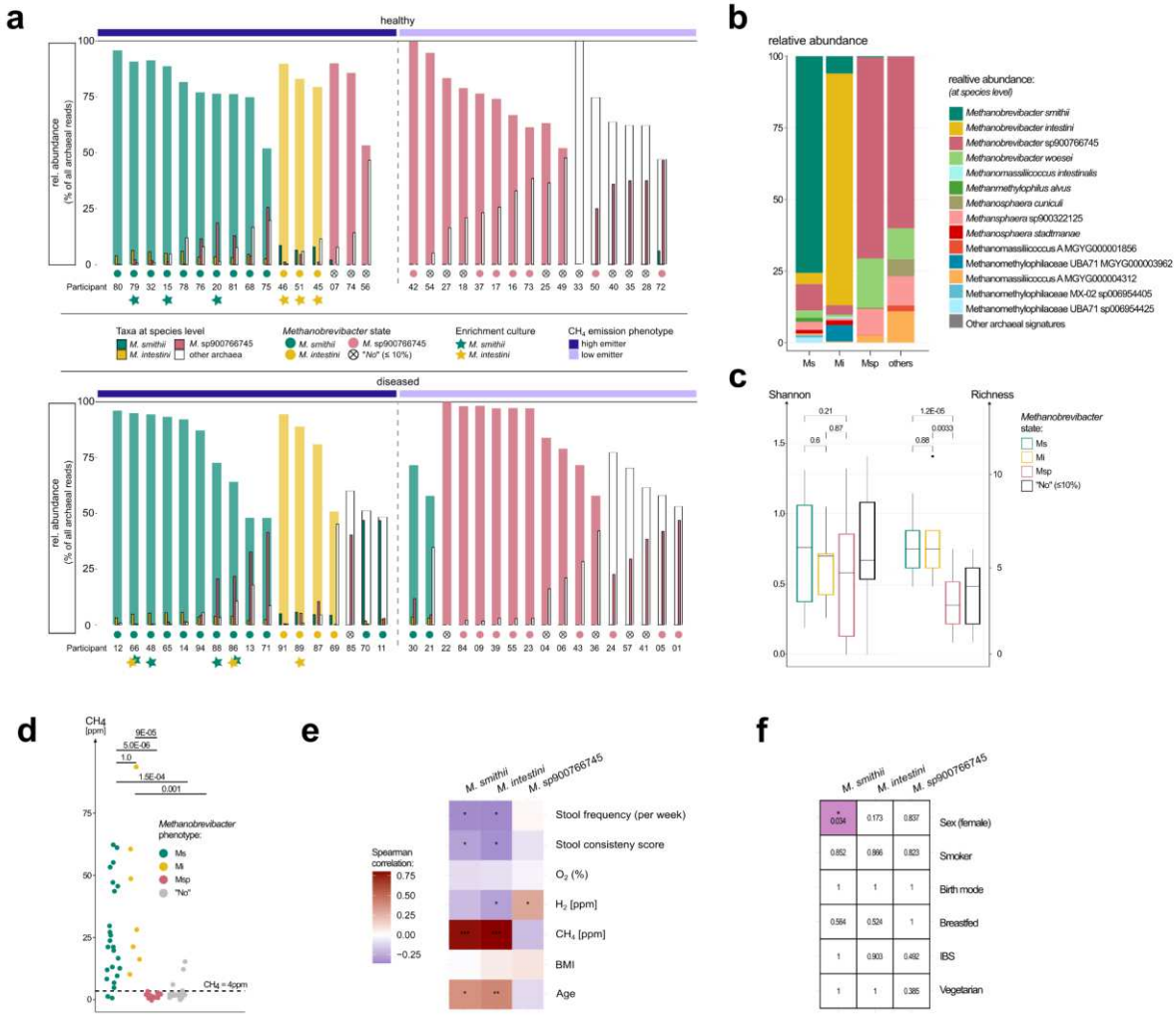
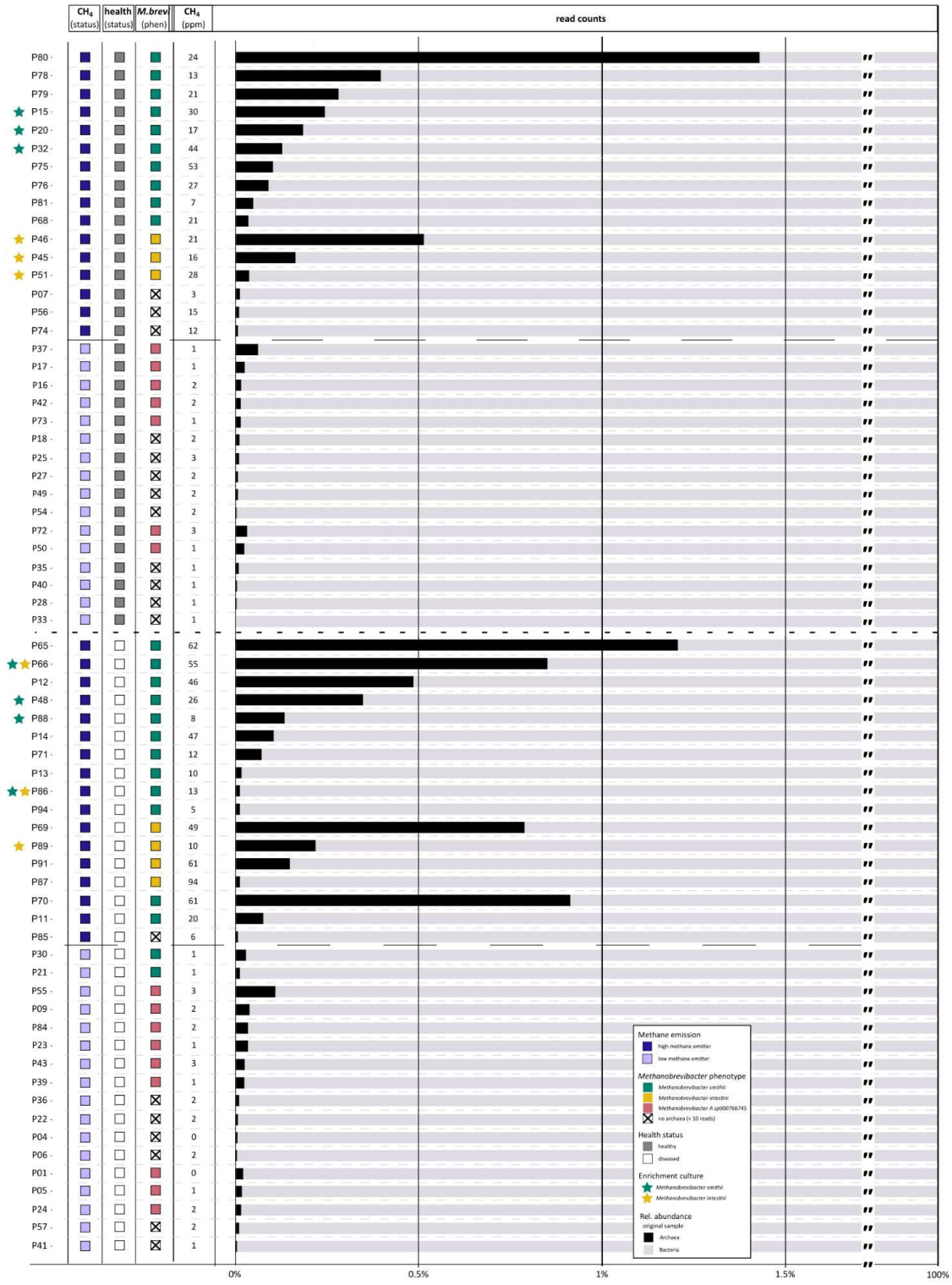
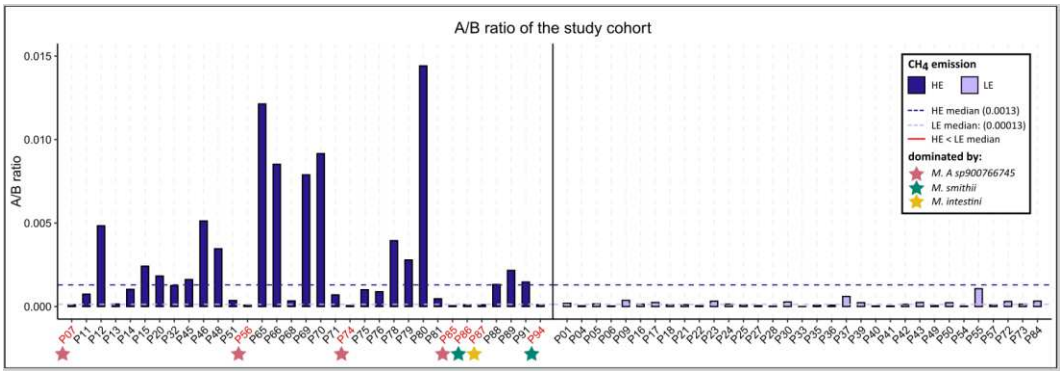


Figure 3. Participants can be categorized into different *Methanobrevibacter*-dominant states. a. Dominant archaeal taxa across high and low methane emitters with identified *Methanobrevibacter*-dominant states. **b.** Top14 archaeal species found in the *Methanobrevibacter* states. **c.** Archaeal richness (but not Shannon diversity) differs between Ms/Mi and Msp/na states. **d.** Significant differences in CH_4 emission between *Methanobrevibacter* states with higher methane emission in Ms and Mi was observed ($p_{MsvsMsp}$ = 5.0E-06; $p_{MivsMsp}$ = 9.0E-05; p_{MsvsNo} = 1.5E-04; p_{MivsNo} = 0.001). **e.** and **f.** Statistics between dominant archaeal taxa and metadata variables showed significant correlations (numerical and categorical; Spearman correlation, Kruskal Wallis test; see also **Supp. Tab. 03**). * p-value < 0.05, ** p-value < 0.01, *** p-value < 0.001



Supp. Figure X4. Relative abundance of archaeal taxa in HE and LE. Data was grouped according to methane emission, health status and *Methanobrevibacter* state. Information was plotted on the left side. Relative abundance of archaeal and bacterial read counts are presented in the right barplot. Stars (☆) indicate samples from which *Methanobrevibacter sp.* were successfully isolated. The plot is based on non-normalized data.



Supp. Fig. X5. Ratio between archaeal and bacterial reads in the samples of our study cohort. In general, HE show a higher A/B ratio compared to LE.

Methanogen states are embedded within distinct fermentative microbiomes

To determine whether different *Methanobrevibacter* states represent broader ecological configurations, we examined bacterial community structure across methane phenotypes and dominant methanogen states. Consistent with previous observations [4], HE microbiomes showed a significantly higher microbial diversity than LE, reflecting a more complex and metabolic versatile ecosystem (**Supp. Fig. X6a**). Although overall microbial community composition overlapped, microbiomes remained significantly segregated by $methane\ phenotype$ (**Supp. Fig. X6b**).

Stratification by $Methanobrevibacter\ states$ (Ms, Mi, Msp and No) revealed similar patterns. Ms and Mi states showed a significantly higher Shannon diversity than Msp and No, driven by increases in both richness and evenness (**Fig. 4a**). Community composition also separated according to archaeome state, with Ms and Mi states more similar to each other than to Msp and No communities (**Fig. 4b**).

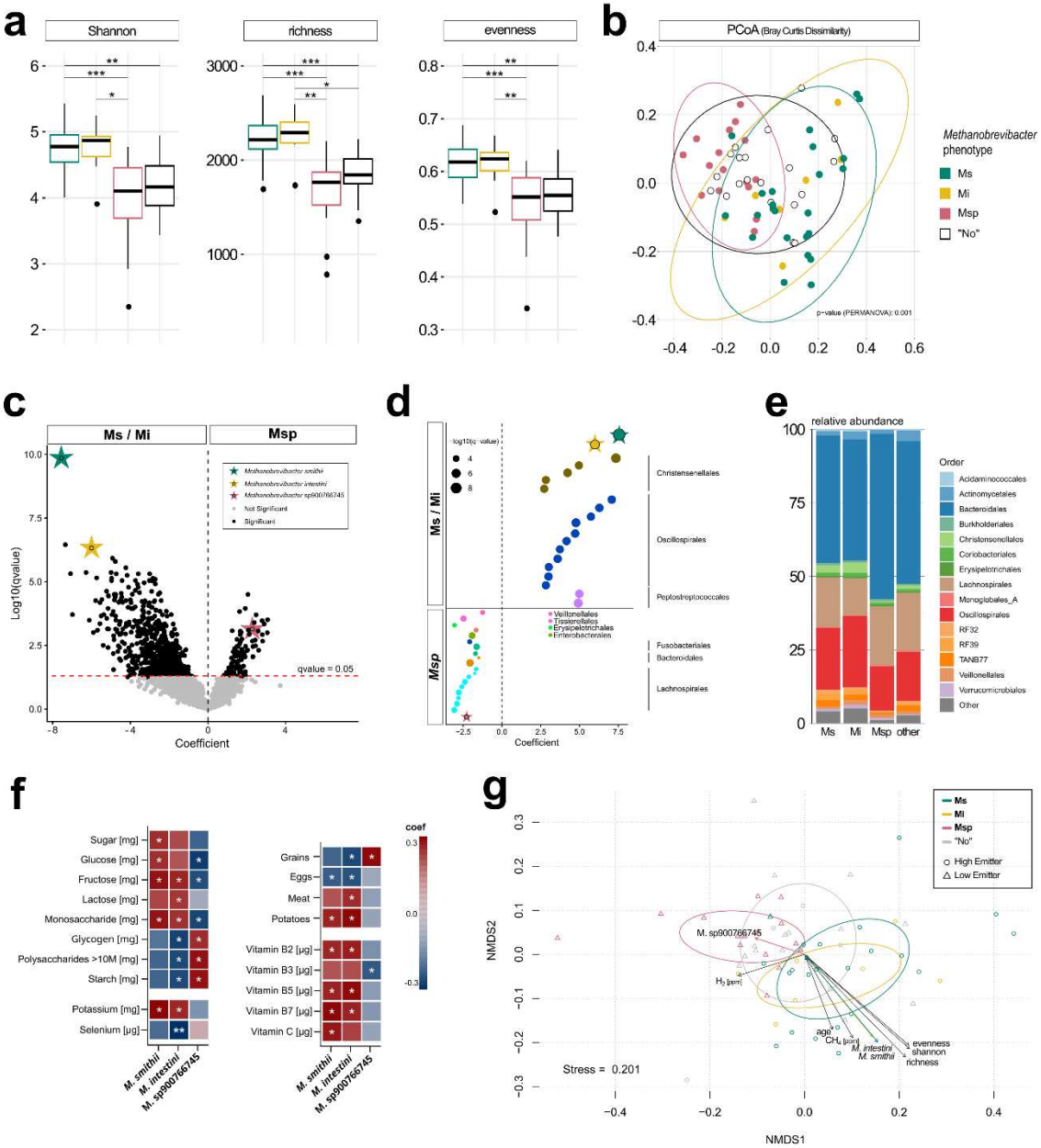
Differential abundance analysis identified distinct bacterial signatures associated with these states. As expected, *M. smithii* and *M. intestini* were the strongest discriminants of the Ms/Mi-associated microbiome ($q = 1.42\ x10^{-10}$ and $q = 4.75\ x10^{-7}$, respectively; MaAsLin2), whereas *M.* sp900766745 was associated with the Msp-state ($q = 0.0007$) (**Fig. 4c** and **4d; Supp. Tab. 04**). At higher taxonomic levels, Ms/Mi were primarily enriched in members of *Christensenellales* (12.7% of the Ms/Mi-associated species; $q = 0.0001$) and *Oscillospirales* (50.8% of the Ms/Mi-associated species; $q = 0.024$), bacterial groups that account for the top 7 bacterial orders and include many fiber-degrading and butyrate-producing lineages, generating acetate, butyrate, and H_2/formate [3,26,27]. In contrast, Msp was predominantly enriched in *Lachnospirales* (42.7% of the LE-associated species, $q = 0.27$) and *Bacteroidales* (24.7% of the LE-associated taxa, $q = 0.026$) (**Fig. 4d** and **4f**), taxa that frequently favor saccharolysis via reduced organic end products (e.g., butyrate, lactate, succinate) or propionate pathways with lower net H_2 output compared to acetate, or H_2-recapturing strategies (e.g., flavin-based electron bifurcation, fumarate reduction) [14]. Similar compositional differences were observed when communities were stratified directly by $CH4\ phenotype$ (**Supp. Fig. X6c and X6d**).

Microbial association networks further supported distinct ecological organization of the archaeome states. *M. smithii* and *M. intestini* occupied partially overlapping networks within the HE microbiomes with associations centered on Oscillospirales and Christensenellales (**Supp. Fig. X6e**).

In contrast, *M.* sp900766745 formed a small and peripheral network in HEs but was centrally positioned within the largest archaeal-bacterial networks within the LEs, enriched in *Bacteroides* (**Supp. Fig. X6e**). These contrasting network structures suggest that the three *Methanobrevibacter* lineages occur within different microbial interaction contexts.

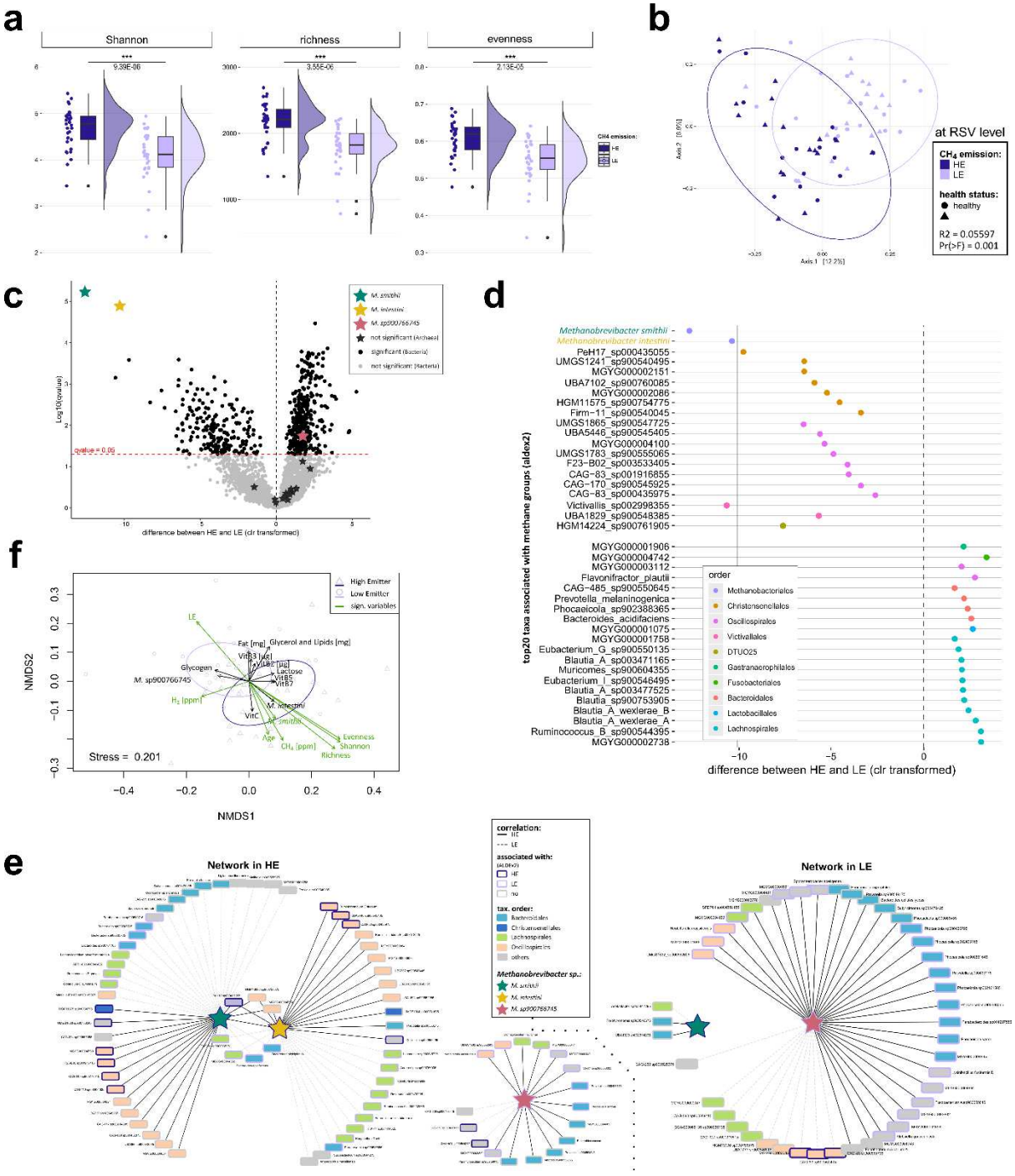
Because substrate availability may influence these community configurations, we next examined dietary intake. Of 142 quantified nutrients, only vitamin B3 differed significantly among individuals classified by dominant *Methanobrevibacter* state, and no dietary variable consistently distinguished the three states. Correlation analyses nevertheless identified positive associations between *M. smithii*, *M. intestini* and the HE state and several carbohydrate and vitamin intakes (glucose, fructose; particularly B-group vitamins and vitamin C), whereas *M.* sp900766745 and LE individuals displayed inverse associations, particularly with grain-derived nutrients and glycogen (**Fig. 4f**, **Supp. Tab. 05**). Dietary variables, however, did not explain the overall microbiome variation (**Fig. 4g**).

These results indicate that $methane\ phenotypes$ are associated with distinct fermentative ecosystems. HE microbiomes are characterized by diverse bacterial communities enriched in hydrogen-generating fermentative taxa that support *M. smithii* and *M. intestini*-associated syntrophy, whereas LE microbiomes represent a lower-diversity, distinct ecological state associated with *M.* sp900766745 and alternative microbial interactions.



362

363 **Figure 4. *Methanobrevibacter* states come with a different microbial community. a.** Alpha diversity across
364 the identified *Methanobrevibacter* states. **b.** Beta diversity **c.** and **d.** Most and top 20 discriminative microbial
365 species between Ms/Mi and Msp states. **e.** Bacterial composition at order level found within the *Methanobrevibacter*
366 states. **f.** Dietary variables found to be significantly different with one of the three dominating *Methanobrevibacter*
367 species (* p-value < 0.05, ** p-value < 0.01, *** p-value < 0.001; see also **Supp. Tab. 05**). **g.** No dietary variable
368 was able to explain variations in microbiome composition. Variables shown here found to be significantly different
369 when correlated with CH_4 level, age, alpha diversity, or *Methanobrevibacter sp.* (Spearman correlation) or emitter
370 status (Mann-Whitney U/t-test); only variables marked in green could explain variations in the microbiome.
371 *Methanobrevibacter* states: "No": Samples in which the overall normalized archaeal reads accounted for <0.01%
372 of the total microbial reads were classified as having no detectable archaeal signal (19/66 samples). Ms, Mi and
373 Msp; *Methanobrevibacter* species: *M. smithii*, *M. intestini*, Msp900766745.



Supp. Fig. X6. **Gut microbiome of HE and LE differs in diversity and bacterial partners.** **a.** Alpha diversity of HE samples was significantly higher compared to LE. (Shapiro-Wilk: Shannon = 0.013; Richness = 0.030; Evenness = 0.009; Mann Whitney U q-value: Shannon = 9.39E-06; Richness = 3.55E-06; Evenness = 2.13E-05) **b.** Microbial communities of the CH_4 emission phenotypes were overlapping but not completely separated (beta diversity; nonSRS data; Permanova - p-value: 0.004) **c.** Differential abundance analysis shows several microbial taxa that are significantly associated with one or the other CH_4 emission phenotype. (ALDEx2: q-value and diff.btw). **d.** Differential abundance analysis of the top 20 taxa associated with either HE or LE. *M.* sp900766745 does not show up in the list of the top 20, however, was still significantly associated with LE. (ALDEx2: q-values; clr-transformed data). **e.** Microbial networks around the three most discriminative archaeal taxa built on HE and LE data, respectively(shotgun, species level; grey lines: negative correlation; black lines: positive. correlation) f. No dietary variable could explain the differences in the microbial communities between the two CH_4 emission states.

Comparative genomics reveals metabolic specialization among human gut Methanobrevibacter lineages

To investigate the genomic basis underlying the distinct ecological niches of the three dominant *Methanobrevibacter* lineages, we compared their genomic repertoires and predicted metabolic capacities. Metagenomic assembly recovered two high-quality *M. smithii* genomes and one *M. intestini* genome, together with 176 high-quality bacterial metagenome-assembled genomes (MAGs; completeness ≥95%, contamination ≤5%), predominantly affiliated with *Clostridia* (102 MAGs) and *Bacteroidia* (28 MAGs) (**Fig. 5a**; **Supp. Fig. X7**; dereplicated *Methanobrevibacter* MAGs can be found here: PRJEB127146). No MAGs of *M.* sp900766745 were recovered. To comparative analyse, we therefore selected 10 representative genomes per *Methanobrevibacter* lineage, prioritizing isolate genomes where available and complementing these with high-quality MAGs (0% contamination; mean completeness 99.5%; **Supp. Tab. 06**).

The three lineages shared a conserved metabolic core but differed substantially in genome architecture and predicted substrate utilization. *M. sp900766745* had the smallest median genome size (1.64 Mbp), compared with *M. intestini* (1.85 Mbp) and *M. smithii* (1.77 Mbp) (**Supp. Tab. 06a**).

Transporter predictions identified conserved capacities for uptake of amino acids and amino acid derivatives, consistent with the importance of host- and microbiome-derived organic substrates for gut-associated methanogens (Mohammadzadeh et al., 2026). In contrast, *M.* sp900766745 lacked several transport systems broadly conserved in *M. smithii* and *M. intestini*, including predicted uptake systems for glycerol, guanosine, nitrite, cyanate, uracil, thiamine, folate and heme. It also uniquely encoded predicted GABA uptake, while 6/10 genomes encoded a maltose transporter (**Fig. 5b; Supp.Tab. 06b-d**). The reduced predicted uptake of nucleosides and other components in *M.* sp900766745 suggests a lower reliance on scavenging these metabolites from the gut environment, potentially reflecting greater metabolic self-sufficiency.

Differences were particularly pronounced in methanogenic substrate flexibility. *M. smithii* and *M. intestini* retained reactions associated with methyl compound utilization, *M.* sp900766745 lacked multiple methyltransferase reactions involved in methanol and methylated cofactor utilization, including methanol-specific methyltransferase components (*MtaA*/*B*/*C*) and methylated *MtbC*, *MtmC* and *MttC* processing reactions (**Fig. 5c**; **Supp. Tab. 06e-g**). Nevertheless, all three lineages retained the essential enzymes required for hydrogenotrophic methanogenesis from CO_2 or formate using H_2 as electron donor (**Fig. 5c**).

Central carbon metabolism was highly conserved among all three lineages. Genes involved in gluconeogenesis, the pentose phosphate pathway and the incomplete TCA cycle were present across *Methanobrevibacter* genomes (exemplarily shown in **Supp. Fig. X8a**), consistent with acetate serving primarily as a carbon source for biomass production rather than energy generation [16]. Stable-isotope probing confirmed that acetate was incorporated into archaeal biomass: isolates of *M. smithii* (from sample P31) and *M. intestini* (from sample P45) actively expressed methanogenesis-associated genes and produced methane. Following incubation with uniformly ^{13}C-labelled acetate, isotope incorporation was detected in anabolic products including amino acids (alanine, glutamate and aspartate), nucleotide-associated metabolites (glycine and serine), and archaeal membrane lipid precursors such as glycerol-3-phosphate (**Fig. 5d; Supp. Fig. X8b**). Add some graphs showing 13C-incorporation as a supplementary figure?

Genome-scale metabolic modeling revealed a highly conserved metabolic core across the analyzed *Methanobrevibacter* strains. All reconstructed models predicted uptake of inorganic nutrients and central carbon and nitrogen sources, including H_2, CO_2, phosphate, ammonia, glucose, acetate, sulfate, methionine, urea, and oxalate, together with the production of methane, formaldehyde, and hydrogen sulfide (**Supp. Tab. 06h**). However, *M.* sp900766745 displayed several lineage-specific features, including predicted dependence on L-phenylalanine uptake, absence of methylsulfide utilization and lack of predicted methanethiol production. In addition, this lineage lacked polyphosphate kinase and exopolyphosphatase reactions, even under relaxed annotation thresholds (**Supp. Tab. 06e**), suggesting altered phosphate storage and stress-response capacities. The absence of formate hydrogenlyase-associated reactions further indicated differences in electron transfer flexibility. Conversely, *M.* sp900766745 uniquely encoded acetylornithine deacetylase, suggesting divergence in ornithine and arginine metabolism.

Flux balance analysis further predicted lower median growth rates and reduced biomass production for *M.* sp900766745 compared with *M. smithii* and *M. intestini* (**Supp. Tab. 06h and 06i**).

Collectively, these comparative analyses suggest that *M.* sp900766745 represents a metabolically specialized *Methanobrevibacter* lineage characterized by reduced substrate flexibility, particularly for methyl compound utilization, combined with distinct adaptations in nutrient acquisition and nitrogen metabolism.

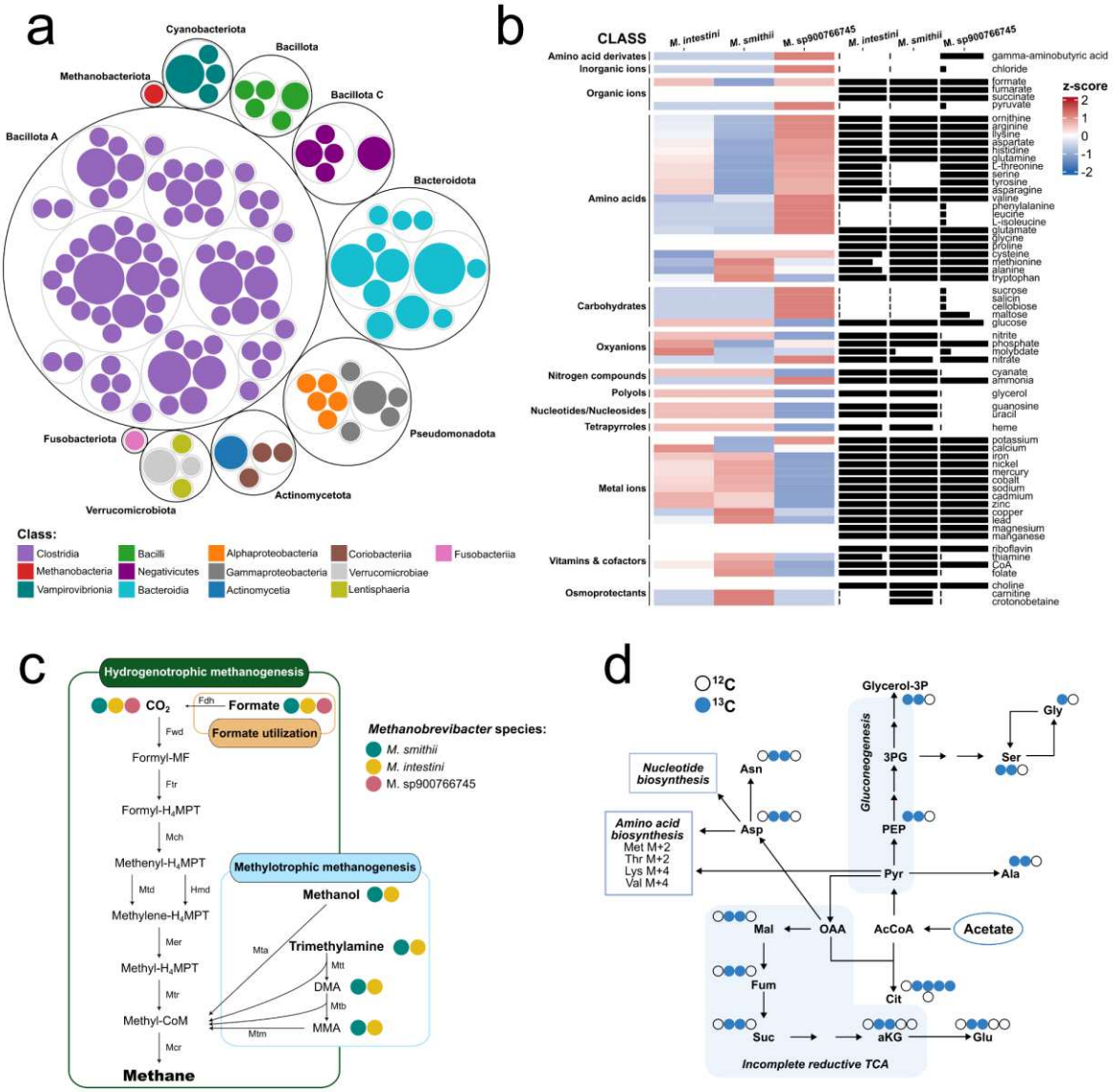
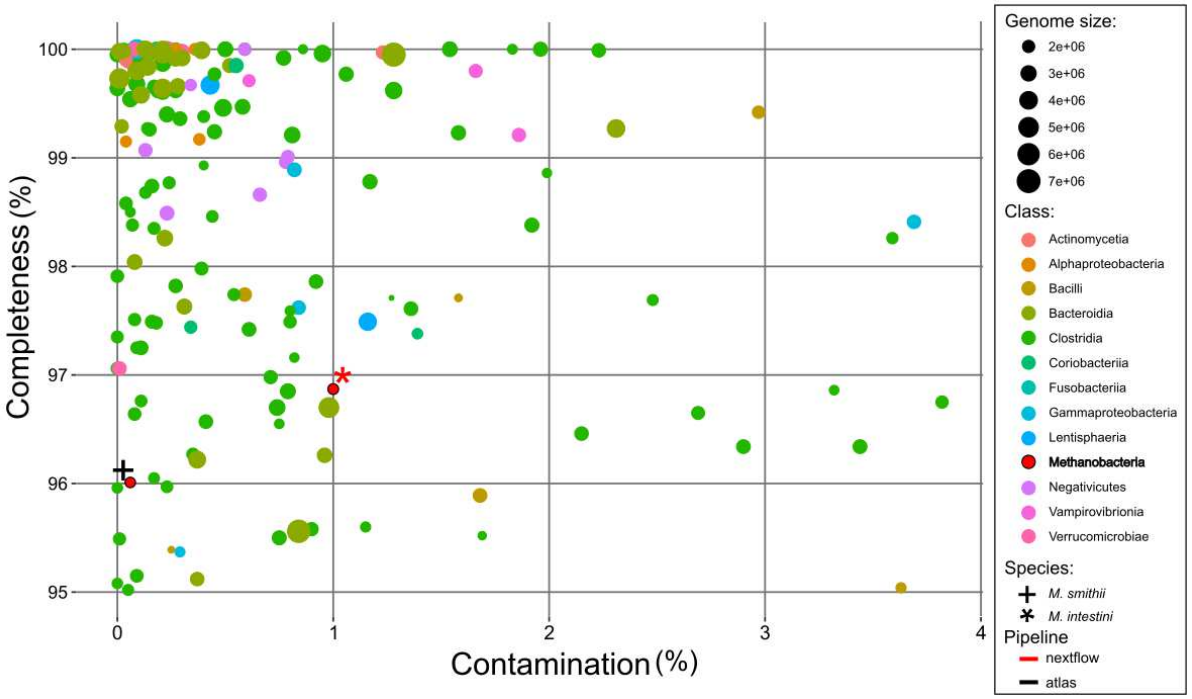
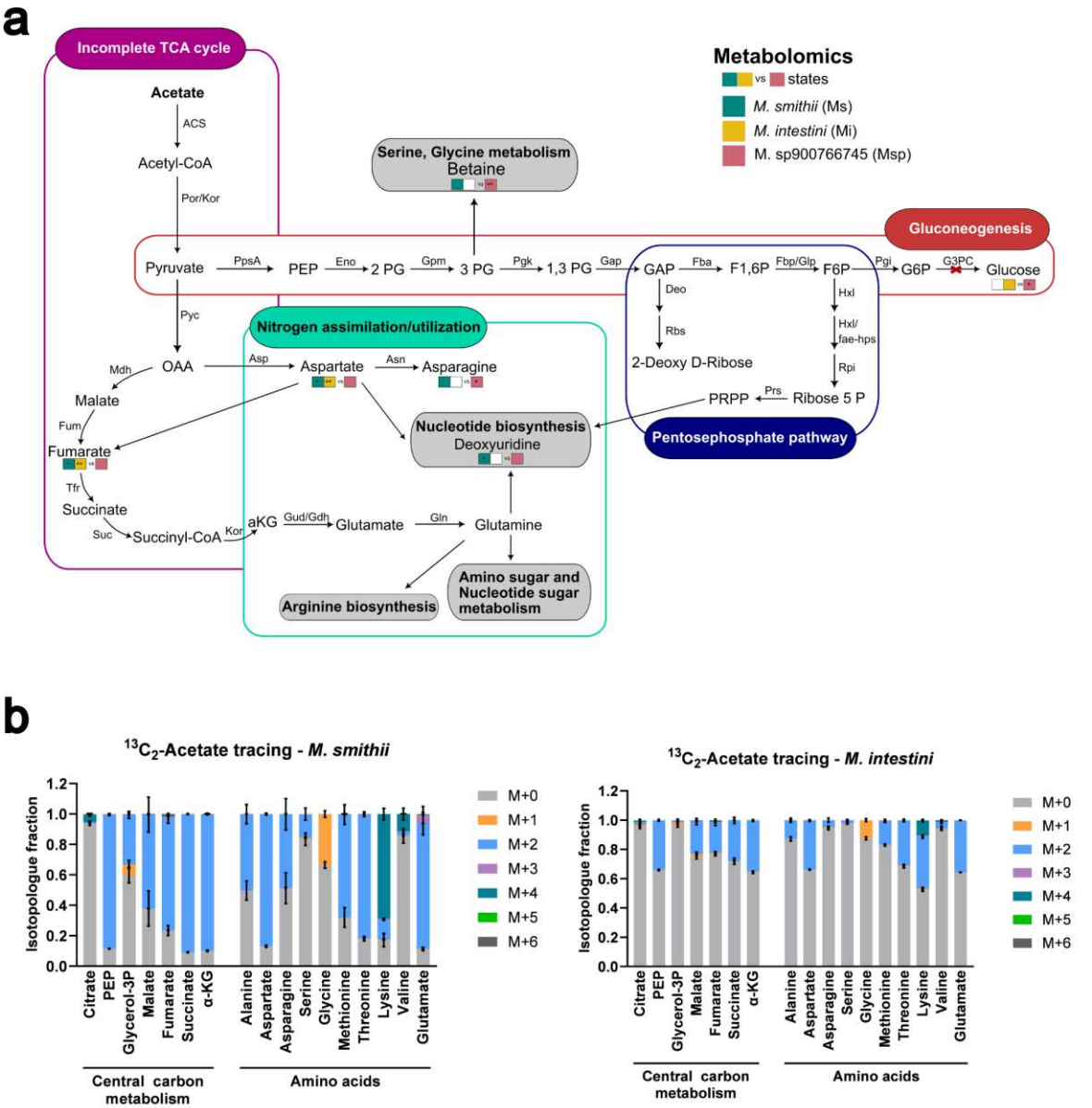


Figure 5. Similar yet distinct energy and biomass metabolism, and transporter capacities predicted from metagenomes and supported by experimental data. a. Metagenomic assembled genomes (MAGs) found in the shotgun data after quality filtering (completeness >95; contamination < 5). Circle size represents the number of MAGs retrieved for each taxonomic class, with larger circles indicating a greater number of MAGs. **b.** Predicted substrate transporters across *Methanobrevibacter* species. Heatmap showing the relative abundance of predicted substrate-specific transporter genes across three *Methanobrevibacter* species groups (10 representative genomes per species). left: Rows correspond to transported substrates and are grouped by substrate type. For some substrates, more than one transporter was predicted; for full details, please see **Supp. Tab. 06**. i) Values represent row-wise z-score scaled mean transporter abundances calculated from presence-absence profiles of individual genomes within each species group (blue to red color scale indicates low to high relative abundance). ii) Right-hand bar annotations indicate transporter presence frequency per species group, defined as the fraction of genomes encoding at least one transporter for the given substrate. Bars are shown separately for each species group, with full-length bars indicating universal presence and shorter bars indicating partial occurrence within the species. **c.** Methanogenesis substrates and pathways identified in three *Methanobrevibacter* species based on retrieved MAGs and representative genomes (10 genomes per species). **d.** ^{13}C-Acetate tracer experiment in monocultures of *M. smithii* and *M. intestini* isolates.



Supp. Fig. X7. Quality of retrieved MAGs of the shotgun data. Two complementary bioinformatic approaches, the metagenome-atlas and nextflow workflows, were used to recover MAGs. However, the Nextflow pipeline was applied only to reads mapped to the *M. intestini* reference genome. Only MAGs with >95% completeness and <5% contamination are shown.



Supp. Fig. X8. **Central carbon metabolism was highly conserved among all three lineages.** **a.** Central carbon metabolism highlighting enzymes identified in genomic and metatranscriptomic data. Metabolites that differed significantly between Methanobrevibacter states based on metabolomic analysis are indicated by colored boxes and asterices. * p-value < 0.05, ** p-value < 0.01, *** p-value < 0.001 **b.** Stable isotope tracing with $^{13}C_2$-acetate in M. intestini and M. smithii. Isotopologue fractions of metabolites in *M. smithii* and *M. intestini* after tracing with 10 mM $^{13}C_2$-acetate for 26 hours (n = 3). Samples were analyzed by gas chromatography-mass spectrometry. OAA, oxalocetate; PEP, phosphoenolpyruvate; Glycerol-3P, glycerol-3-phopshate; α-KG, α-ketoglutarate; 2 PG, 2-phosphoglycerate; 3 PG, 3-phosphoglycerate; 1,3 PG, 1,3-bisphosphoglycerate; GAP, glyceraldehyde 3-phosphate; F1,6P, fructose 1,6-bisphosphate; F6P, fructose 6-phosphate; G6P, glucose 6-phosphate; PRPP, 5-phosphoribosyl-1-pyrophosphate.

Low methane emitters are characterized by incomplete fermentation and lower microbiome activity

To determine whether the distinct *Methanobrevibacter* lineages identified above also differ in their functional impact on the gut ecosystem, we integrated stool metabolomics with community-wide metatranscriptomics.

Untargeted stool metabolomics demonstrated clear distinct metabolic profiles across archaeome states (**Supp. Data. 06**). Communities dominated by *M. smithii* (Ms) and *M. intestini* (Mi) contained significantly higher concentrations of metabolites associated with advanced anaerobic carbon metabolism, aromatic amino acid degradation and nucleotide turnover, including fumaric acid (Ms: q = 0.011; Mi: q = 0.006), deoxyuridine (Ms: q = 0.014) and aspartic acid (Ms: q = 0.028). In contrast, archaeomes dominated by *M.* sp900766745 (Msp) contained higher levels of comparatively unprocessed substrates, including glucose (Msp: q = 0.032) and asparagine (Msp: q = 0.013) (**Fig. 6a**; **Supp. Tab. 07**), suggesting reduced downstream microbial substrate conversion. The measured short-chain fatty acids (SCFAs), including acetic, butyric, and propionic acid, did not differ significantly between groups. However, the relative proportions of individual SCFAs showed trends for butyric (↑Msp) and propionic acid (↓Msp) (**Supp. Fig. X9**)

To link these functional capacities and metabolite patterns to active microbial processes in stool samples, we next profiled community-wide gene expression using stool metatranscriptomics (**Supp. Data 05**). Differentially abundant transcripts were primarily associated with two major functional categories: energy metabolism and genetic information processing, with the largest transcriptional shifts observed in Mi-associated communities (**Fig. 6b-d**).

Given the central role of methanogens as hydrogen sinks, we specifically examined transcripts involved in hydrogenotrophic methanogenesis and electron transfer. Specifically, *Mi* and *Ms* states were dominated by ***methanogenesis***-involved transcripts tied to H_2 oxidation and downstream electron flow particularly oxidoreductases (e.g., frh) and electron transport-associated proteins, including multiple dehydrogenases (e.g., fwd, fdh) and reductase families (e.g., hdr) - indicating strong hydrogenotrophic flux from H_2 to CH_4 (**Fig. 6b**; **Supp. Tab. 08**). These genes collectively catalyze hydrogen oxidation, electron transfer and the final reduction steps leading to methane formation, indicating increased hydrogenotrophic flux in the high-methane-associated archaeome states.

Importantly, core methanogenesis genes were detected across all phenotypes, demonstrating that the canonical methane-producing pathway is broadly conserved *in vivo*. Instead, the key differences were observed in supporting redox and energy-transduction transcripts that regulate H_2 uptake, electron bifurcation, and overall efficiency of CH_4 production under varying environmental conditions/in different microbial communities (**Fig. 6b**, **Supp. Tab. 08**).

Beyond energy metabolism, Mi-associated communities also exhibited higher expression of genes involved in **genetic information processing**, as well as ***signaling, motility and transporter transcripts*** (e.g., flagellar proteins, pili-associated proteins and multiple transporter families; ribosomal proteins, transcription-associated factors and DNA replication and repair proteins) (**Fig. 6b**). These differences are consistent with a greater overall biosynthetic and cellular activity. Although these pathways are universally required for cellular function, their increased expression suggests elevated overall biosynthetic activity within Mi-associated communities rather than pathway-specific metabolic specialization. In contrast, transcripts associated with the ***incomplete TCA cycle*** were not differentially expressed between archaeome states (**Supp. Tab. 08**), supporting a broadly conserved central metabolic backbone.

Msp-associated communities exhibited no differentially abundant transcripts, supporting the view that this archaeome state represents a metabolically less active ecosystem characterized by reduced hydrogen turnover and shallower fermentation (**Fig. 6d**; **Supp. Tab. 08**).

Together with the metabolomic profiles, these results indicate that the three *Methanobrevibacter* states correspond to distinct functional configurations of the gut microbiome. *Ms* and Mi states are associated with greater hydrogenotrophic methanogenic activity and more extensive downstream substrate conversion, whereas the Msp state is characterized by accumulation of residual substrates and lower detectable community-wide transcriptional activity.

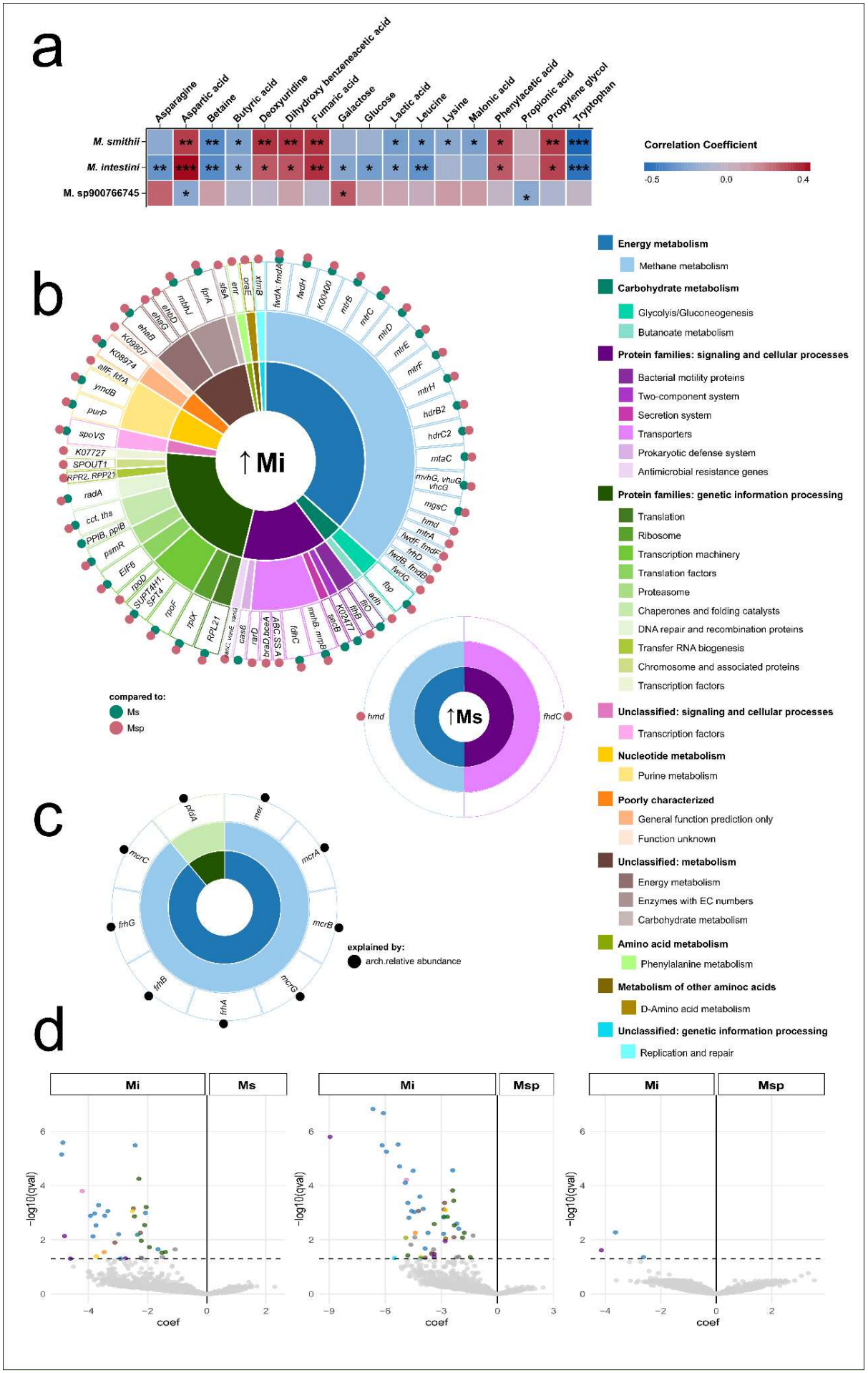
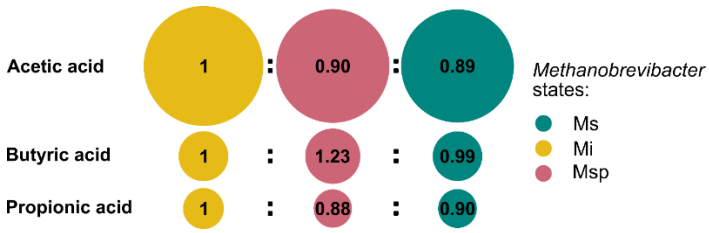

a
Asparagine
Aspartic acid
Betaine
Butyric acid
Deoxyuridine
Dihydroxy benzeneacetic acid
Fumaric acid
Galactose
Glucose
Lactic acid
Leucine
Lysine
Malonic acid
Phenylacetic acid
Propionic acid
Propylene glycol
Tryptophan
M. smithii
M. intestini
M. sp900766745
Correlation Coefficient
-0.5
0.0
0.4
b
↑Mi
↑Ms
compared to:
Ms
Msp
Energy metabolism
Methane metabolism
Carbohydrate metabolism
Glycolysis/Gluconeogenesis
Butanoate metabolism
Protein families: signaling and cellular processes
Bacterial motility proteins
Two-component system
Secretion system
Transporters
Prokaryotic defense system
Antimicrobial resistance genes
Protein families: genetic information processing
Translation
Ribosome
Transcription machinery
Translation factors
Proteasome
Chaperones and folding catalysts
DNA repair and recombination proteins
Transfer RNA biogenesis
Chromosome and associated proteins
Transcription factors
Unclassified: signaling and cellular processes
Transcription factors
Nucleotide metabolism
Purine metabolism
Poorly characterized
General function prediction only
Function unknown
Unclassified: metabolism
Energy metabolism
Enzymes with EC numbers
Carbohydrate metabolism
Amino acid metabolism
Phenylalanine metabolism
Metabolism of other aminoc acids
D-Amino acid metabolism
Unclassified: genetic information processing
Replication and repair
c
explained by:
arch.relative abundance
d
Mi
Ms
Msp
-log10(qval)
coef

Figure 6. ***M. intestini* and *M. smithii* states differ from Msp state in metabolomic and metatranscriptomic profile.** **a.** Correlation between stool metabolites and *Methanobrevibacter* species (spearman correlation). **b.** Significant different transcripts between *Methanobrevibacter* states (MaAsLin2). **c.** Significant differences based on archaeal relative abundance (MaAsLin2). **d.** Overview on the amount of significantly different transcripts between the three *Methanobrevibacter* states (metatranscriptomics data normalized by count per million and log transformed).



Supp. Figure X9. ***SCFA ratios between the Methanobrevibacter states.*** Ratios of acetic, butyric, and propionic acid concentrations across *Methanobrevibacter* states calculated from the mean metabolite concentrations for each *Methanobrevibacter* state.

DISCUSSION

The gastrointestinal ecosystem is shaped by numerous host factors, including intestinal transit, diet, immune interactions and the mucus layer, together with the metabolic activities and interactions of its resident microorganisms [28–31]. We were interested in gaining deeper insights into the inter-individual differences of methane-production within the colon, and analyzed the species-level contribution of different methanogenic archaea, and put this in context with the host- and bacterial environment. For a long time, gut methane production has been attributed predominantly to *M. smithii*, considering that the gut methanogens form a functionally homogenous group and that genus-level abundance is sufficient to explain variations in methane emission via breath. Here we show that three different, recurrent *Methanobrevibacter* states, characterized by a dominance of three different species (i.e., *M. smithii*, *M. intestini* [23], and uncultivated *M.* sp900766745 [24] are associated with variation in methane and hydrogen phenotypes, bacterial community structure and levels of microbial activity, with influence on the entire gut ecosystem.

The previously less considered *M.* sp900766745 predominated in methane-low emitters (LE; Msp state), but interestingly persisted at low abundance also in high-emitter (HE) individuals, which were usually predominated by *M. smithii* (Ms state) or *M. intestini* (Mi state). Comparative genomics revealed a conserved metabolic core of hydrogenotrophic methanogenesis across the three lineages, but a more restricted substrate-acquisition and metabolic repertoire for M. sp900766745. Most notably, this lineage lacks methylotrophic capacities, which may have consequences beyond methane production as methylated compounds can connect methane metabolism to host-associated metabolic pathways. *M. smithii* has been reported to consume trimethylamine (TMA) and reduce TMAO (trimethylamine N-oxid) levels in mice and humans by this activity [32–34]. Given the association of TMA and TMAO with cardiovascular risk and epithelial damage (e.g., inflammation, mucosal damage) in the colon and rectum, links its presence to potentially beneficial host effects [32,35,36]. This is further in agreement with the predicted L-carnitine and crotonobetaine transporters for *M. smithii*.

Genomic features further point to niche-specific adaptation of *M.* sp900766744. It encodes a predicted γ-aminobutyric acid (GABA) transporter absent from the other species' genomes. In gut microbes, GABA cycling supports acid-stress tolerance by consuming intracellular protons [37–39]. Together with other genome peculiarities, such as additional predicted transporters for carbohydrates which are usually depleted in distal colon (dependent on fiber intake)[40], we predict that *M.* sp900766745 is rather adapted to small intestinal regions or the proximal colon, and does not share an ecological niche with *M. smithii* and *M. intestini*.

The apparent absence of *M.* sp900766745 from our cultivation collection and its low abundance in some high-methane samples also highlight an important limitation of stool-based profiling. Stool predominantly samples the distal luminal compartment and may underrepresent organisms associated with the mucosa or more proximal gastrointestinal regions [41,42]. Direct sampling along the gastrointestinal tract will be required to test this assumption.

Given its distinct genomic characteristics and species-level divergence from other *Methanobrevibacter* lineages (ANI 79.03% to *M. smithii* and ANI 78.99% to *M. intestini* [43]), we propose the name '*Candidatus* Methanobrevibacter hominipaucus sp. nov.' (ho.mi.ni.pau'cus; L. n. homo -inis, a human being; L. adj. paucus, few/small numbers; N.L. masc. adj. hominipaucus, in small numbers in humans; representative genome: MGYG-HGUT-00522).

Gastrointestinal transit provides a plausible link between host physiology to the observed methanogen states. Multiple studies have consistently associated higher methane emission with slower gastrointestinal transit and constipation phenotypes [8,44–47], whereas shorter transit has been associated with less efficient microbial fermentation [28,48]. Our data support these associations: high-emitting Ms/Mi states were characterized by lower stool frequency and firmer stools, whereas LE, Msp states were associated with higher stool frequency and softer stools. Longer residence times increase the opportunity for sequential microbial metabolism and may sustain the availability of substrates and H_2 for hydrogenotrophic methanogens [28,48]. Consistent with this interpretation, Ms/Mi communities showed higher expression of methanogenesis-associated genes, and *M. intestini* was associated with lower breath H_2 than *M.* sp900766745, suggesting more effective H_2 removal in the former or less H_2 demand in M. sp900766745. The higher growth rates observed for *M. intestini* compared with *M.* sp900766745 may further indicate more efficient coupling between H_2 availability and methanogenic energy conservation.

Transit time can also alter the temporal and physicochemical conditions under which microbial metabolism occurs. Along the gastrointestinal tract, complex carbohydrates and other substrates are progressively fermented to SCFAs, which are subsequently absorbed [49,50]. Further distally, readily fermentable carbohydrates and free SCFAs become less abundant, while amino acid fermentation becomes increasingly important and generates more alkaline metabolites, contributing to a transition from relatively acidic toward neutral or mildly alkaline conditions [51,52].

Faster transit may interrupt this sequence, by increasing the delivery and retention of incompletely processed substrates while reducing the time available for microbial cross-feeding and host absorption [51]. It may consequently alter the supply of CO_2 and H_2 available

for hydrogenotrophic methanogenesis. The elevated breath H_2 and accumulation of glucose and other incompletely processed substrates observed in Msp-dominated states are consistent with such reduced downstream substrate conversion, whereas the increased *M. smithii* and *M. intestini* abundance and their activity towards the distal colon is compatible with an environment in which prolonged microbial processing has depleted alternative substrates while maintaining fermentation [53].

The three archaeal states were accompanied by distinct bacterial communities, indicating that species-resolved methanogen composition is embedded within a broader microbiome configuration. Msp-associated communities contained several taxa characteristic of saccharolytic metabolism, including Lachnospirales, *Bacteroides* and *Eubacterium* species These organisms rapidly ferment carbohydrates to SCFAs, while limited residence time and incomplete cross-feeding may restrict subsequent conversion and absorption [29,48,49]. Acidification can favor butyrate-producing organisms, including *Eubacterium*, *Faecalibacterium* and *Roseburia*, whereas propionate production may be comparatively reduced under more acidic conditions and slower transit [48,54]. Consistently, the relative propionate fraction was higher in Ms and Mi than in Msp, reflected in ratios of 1:0.902:0.878 (Mi:Ms:Msp). These measurements align with differences in the fermentation environment, although fecal SCFA ratios alone cannot determine luminal pH.

In contrast, the slower transit characteristic of Ms and Mi states coincided with enrichment of fiber-degrading Bacillota (formerly Firmicutes), including Oscillospirales, particularly Ruminococcaceae, and Christensenellales, which have been repeatedly reported to co-occur with *Methanobrevibacter* [4,9]. In the presence of *M. smithii*, Christensenellales can release CO_2, H_2 and formate during degradation of resistant starches and complex polysaccharides and have been associated with a shift in SCFA production from butyrate toward acetate [3,55]. Ms/Mi-associated Enterobacteriales likewise produce acetate, together with formate and other fermentation products [56]. The resulting acetate-rich fermentation environment is consistent with the importance of acetate as a carbon source for *Methanobrevibacter* biomass formation [16].

Our experimental data provide a direct biochemical link between this bacterial fermentation output and archaeal metabolism. $^{13}C_2$-acetate tracing demonstrated incorporation of acetate [57] into multiple metabolites in *M. smithii* and *M. intestini* isolates, while metabolic reconstruction identified acetate utilization capacity across all three *Methanobrevibacter* lineages. Thus, acetate produced during bacterial fermentation represents an important carbon source directly supporting archaeal biomass formation and provides a functional connection between community-level fermentation and methanogen growth.

The SCFA patterns are further compatible with pH-controlled fermenter studies showing that butyrate predominates at pH 5.5, whereas the acetate:butyrate ratio reverses around pH 6.5 [54]. In our cohort, the fecal butyrate ratio between the groups was indeed higher in the Msp state compared to Mi and Ms (1:0.991:1.228), consistent with greater relative butyrate production under the putatively more acidic Msp fermentation regime. However, fecal SCFA concentrations represent the balance between production and epithelial absorption and capture only a fraction of the total colonic SCFA pool [57]. These measurements therefore provide evidence for differences in fermentation output but cannot by themselves resolve the spatial or pH gradients underlying them.

Differences in fermentation output were accompanied by broader differences in substrate turnover, suggesting that the methanogen states may represent different depths of anaerobic metabolism. Slower transit in Ms and Mi states provides additional time for sequential carbohydrate utilization and subsequent metabolism of alternative substrates, including amino acids. From a thermodynamic perspective, hydrogenotrophic methanogens, sulfate-reducing bacteria (SRB) and reductive acetogens can maintain low H_2 partial pressures, allowing otherwise unfavorable H_2-producing reactions to proceed [58,59]. Efficient hydrogen disposal may therefore facilitate continued fermentation and increase the extent to which complex substrates are progressively degraded.

Several observations are consistent with such a shift in Ms and Mi-associated ecosystems. High-CH_4 microbiomes and our Ms/Mi states showed signatures of increased protein turnover and aromatic amino acid metabolism, together with enrichment of secondary protein degraders such as Peptostreptococcales (Anaerovoracaceae), and Enterobacteriales, of which some have been shown to convert amino acids and proteolysis products into acetate, butyrate, ammonia and other metabolites [50,60]. These findings suggest that prolonged microbial processing may extend beyond carbohydrate fermentation toward increased protein fermentation once readily available carbohydrates become depleted. The potential physiological relevance is notable because products of protein fermentation, including ammonia, phenol and p-cresol, have been associated with adverse effects on colonic epithelial cells [61–63]. Thus, the association between slow transit, high methane emission and Ms/Mi states may represent a broader metabolic configuration characterized by more extensive downstream substrate conversion, including proteolysis. Whether this shift is driven primarily by methanogen-mediated hydrogen removal, prolonged transit, bacterial community composition, or their combination remains unresolved.

The contrasting Msp state provides a complementary model. Its reduced activity for hydrogen-dependent methanogenesis and association with higher breath H_2 are consistent with lower

hydrogen-consuming capacity. Elevated H_2 could constrain some hydrogen-producing reactions and contribute to the accumulation of incompletely processed substrates observed in Msp-dominated individuals. Alternative electron sinks may consequently become more important. The association with acetogens such as Blautia is consistent with this possibility, as reductive acetogenesis redirects reducing equivalents toward acetate rather than methane. Methanogenesis generally provides a greater energetic yield than acetogenesis under favorable H_2 concentrations and can therefore competitively exclude acetogens when efficient hydrogenotrophic methanogens such as *M. smithii* are abundant [58,64–66]. Nevertheless, our data do not establish a causal hierarchy in which reduced methanogenesis directly produces the Msp bacterial community. Rather, they support a model in which alternative hydrogen sinks contribute to, and potentially stabilize, distinct fermentation states.

The positive sample-level association between Ms/Mi states and SRB, including Desulfovibrionaceae, provides an additional indication that hydrogen metabolism may be organized spatially along the gut. This association should not be interpreted as evidence for relaxed competition or local cohabitation within the same microniche. Instead, it may reflect longitudinal metabolic partitioning: H_2 and CO_2 production increases toward the distal colon by bacterial fermentation, providing a potential substrate for hydrogenotrophic taxa. However, SRB can also use organic electron donors such as lactate, ethanol, pyruvate, etc., so their distribution isn't determined by H_2 alone [67], whereas methanogens may become more competitive distally as they rely on H_2 and use CO_2 [16,59,68]. Moreover, under sulfate limitation, one gut SRB, namely *Desulfovibrio vulgaris*, can ferment organic acids and alcohols to H_2, and CO_2 in bioreactors [69,70], potentially functioning also in the gut as upstream producers rather than hydrogen sinks. The observed co-association could therefore represent a spatial and metabolic relay, in which proximal fermentation and sulfate reduction generate substrates that support distal hydrogenotrophic methanogenesis, rather than direct ecological cohabitation.

Taken together, the genomic, physiological and community-level observations support a model, in which *Methanobrevibacter* lineages occupy partially distinct ecological niches along the gastrointestinal tract. Msp combines a restricted metabolic repertoire, distinctive carbohydrate transport capacity, a predicted GABA transporter, elevated H_2 and low methane emission, whereas Ms and Mi show greater methanogenic activity, broader substrate utilization and stronger associations with fiber-degrading and acetate-producing bacterial communities. These features are consistent with different physicochemical and substrate regimes along the gastrointestinal tract, potentially shaped by transit, pH, substrate depletion and competing electron sinks.

We emphasize, however, that spatial partitioning remains a hypothesis rather than a demonstrated property of the three lineages. Our primary measurements were obtained from stool and therefore predominantly represent the distal luminal community. Likewise, fecal SCFA profiles provide an integrated endpoint of production and absorption rather than direct measurements of local fermentation or pH. Direct sampling of mucosal, small-intestinal, proximal and distal colonic communities, ideally combined with spatially resolved measurements of H_2, pH, SCFAs and substrate availability, will be required to test whether the three *Methanobrevibacter* states correspond to distinct anatomical niches. Such studies may also determine whether low stool abundance of Msp reflects genuinely low population size or preferential localization outside the sampled compartment.

Several limitations should be considered. Although the cohort was carefully phenotyped and sampling and bioinformatic procedures were standardized, its size and clinical heterogeneity limit the resolution with which host factors can be separated from microbial effects. Dietary information likewise does not capture all habitual exposures, including potentially relevant supplementation, and residual dietary variation may contribute to differences in microbial composition and activity. More fundamentally, most ecological associations were derived from cross-sectional stool samples and therefore cannot establish temporal relationships or causality between transit, methanogen composition, bacterial community structure and methane production.

The functional interpretation of *M.* sp900766745 is also necessarily more tentative than that of *M. smithii* and *M. intestini.* Its metabolic properties were inferred primarily from genome-resolved analyses because we were unable to obtain an isolate. Isolation and cultivation will therefore be an important next step for experimentally testing its predicted substrate dependencies, methylotrophic deficiency, hydrogen metabolism and response to pH or GABA availability. Defined co-cultures and synthetic communities could further establish whether differences in H_2 transfer, acetate exchange and competition with alternative electron sinks are sufficient to reproduce the observed ecosystem states. Finally, spatially resolved sampling and host-associated experimental systems, including intestinal organoids, could determine whether species-specific methanogen metabolism alters epithelial responses or other host phenotypes.

Conclusion

Our findings expand the interpretation of human gut methane production from a measure of methanogen abundance to a species-resolved ecological phenotype. Three recurrent *Methanobrevibacter* states were associated with distinct host transit characteristics, bacterial

fermentation communities, hydrogen phenotypes, genomic capacities and levels of microbial activity. The convergence of these observations suggests that hydrogen availability provides an important ecological link between host physiology, bacterial fermentation and archaeal metabolism: fermentation generates H_2, methanogens consume it, and the resulting hydrogen balance can influence the thermodynamic landscape and depth of anaerobic carbon turnover.

More broadly, methane emission may therefore serve as a non-invasive readout of alternative configurations of the gut microbial ecosystem. Species-level resolution is essential to this interpretation, because closely related methanogens can differ substantially in substrate utilization, hydrogen metabolism and ecological niche. Resolving this previously underappreciated archaeal diversity provides a basis for understanding how host physiology and microbial interactions jointly shape methane production and, potentially, broader metabolic and host-associated phenotypes.

Acknowledgements

We thank the participants of the study for their valuable contributions, including donation of microbial material and completing the study questionnaires.

This research was funded in whole or in part by the Austrian Science Fund (FWF) [10.55776/P32697 (given to C.M.E.), excellence cluster “Microbiomes Drive Planetary Health” 10.55776/CoE7 (C.M.E., C.D.), and SFB ImmunoMetabolism 10.55776/F8300 (C.M.E.)]. C.M.E. has received funding from the European Research Council (ERC) under the Horizon Europe research and innovation program (Project ID 101199346, ERC-2024-ADG). We gratefully acknowledge the computational resources provided by the MedBioNode at the Medical University of Graz, funded by the Austrian Federal Ministry of Education, Science, and Research through the Hochschulrat-Struktur Mittel 2016 grant within BioTechMed Graz. We also thank the ZMF Core Facility Computational Bioanalytics team at the Medical University of Graz for their support. S.D. and M.B. were supported by the local doctoral programs MolMed (Medical University of Graz). We thank Rafael Regnet da Cruz for digitalizing the dietary data.

Madl lab: We thank the Center for Medical Research, Medical University of Graz for laboratory access. T.M. is grateful to the Austrian Science Fund (FWF) for excellence cluster 10.55776/COE14, Grants DOI 10.55776/DOC130, 10.55776/P28854, 10.55776/I3792, and 10.55776/W1226, the Austrian Research Promotion Agency (FFG) grants 864690 and 870454; the Integrative Metabolism Research Center Graz; the Austrian Infrastructure Program 2016/2017; the Styrian Government (Zukunftsfonds, doc.fund program, COE14); the City of Graz (doc.fund program, COE14); and BioTechMed-Graz (flagship project). This project was funded in part by the FFG and the European Union (EFRE) under grant 912192. For the purpose of open access, the authors have applied a CC BY public copyright licence to any author accepted manuscript version arising from this submission.

Authors’ contributions

MB and SD recruited the participants and were supported by LS, CH and AMM Sample preparation, DNA and RNA extraction were performed by SD, LS, SV. CK and CME performed data analysis and created most of the shown figures and tables. SL and SH provided digitalized dietary indices. RM performed gapseq analysis. Samples for tracer experiment were cultivated by TZ, and GC-MS and data analysis were performed by TH and

KL. HH and TM performed NMR sample preparation, measurements and metabolomics data analysis. AM and CD provided tools and workflows used in this study, and valuable feedback on the data analysis and manuscript. CME initiated and designed the study. A.M. was involved in planning and implementation of the study. CK and CME wrote the manuscript. The authors critically read and approved the final manuscript.

Correspondence: CME

Competing interests:

All authors declared no competing interests.

Data availability

Quality-filtered raw sequencing data obtained from shotgun metagenomics- and metatranscriptomics- based sequencing (human reads were removed) obtained in this study can be found in the European Nucleotide Archive (ENA): PRJEB127146. Metadata, feature tables and results of shotgun metagenomics-, metatranscriptomics- and metabolomics-based data as well as a list of all MAGs can be found in the **Supp. Data 01-06 and Supp. Tables 01-10** (https://github.com/CME-lab-research/AGAD/). Additionally, *fasta.gz* files of the retrieved *Methanobrevibacter* MAGs were uploaded to the ENA database (PRJEB127146).

Material and Methods (3000 words)

Cohort and Ethics

Eighty participants, aged 20 to 78 years, with varying health conditions (either healthy or experiencing gastrointestinal disease and/or symptoms, such as food intolerances, inflammatory bowel disease or irritable bowel syndrome), were recruited based on their baseline breath methane (CH_4) levels (≥4 ppm, classified as high CH_4 emitters). Medical doctors at the State Hospital in Graz, Austria, along with an independent physician in Graz, Austria, supported the recruitment process.

Each participant provided a stool sample for microbiome analysis, underwent a breath test to measure CH_4 emissions, and completed a questionnaire covering general information, health status, and dietary habits (**Supp. Tab. 01**). Prior to participation, all individuals signed informed consent. Details on inclusion and exclusion criteria are available in **Supp. Tab. 09**. The study received approval from the local ethics committee at the Medical University of Graz, Austria (EK-Nr: 31-452 ex 18/19).

Classification based on methane emission - high and low methane emitters

Breath methane emission of all participants was assessed to group the cohort based on the methane emission phenotype. Participants with breath CH_4 levels ≥4 ppm were classified as high CH_4 emitters based on the criteria in [4]. Depending on availability, individuals either performed the test directly using the GastroCH4ECK™ Gastrolyzer (Bedfont Scientific Ltd., UK) or collected their breath samples in a GastroCH4ECK™ breath bag (Bedfont Scientific Ltd., UK) for later analysis with the Gastrolyzer device. All measurements were performed following the manufacturer's instructions. Measured CH_4 emission in parts per million can be found here: **Supp. Tab. 01**.

Nutritional assessment

Participants' dietary habits and food intake over the four weeks prior to the study were evaluated with the validated German Food Frequency Questionnaire (FFQ) from the Robert Koch Institute [71]. Nutrient composition including the average intake of a comprehensive set of macro- and micronutrients (e.g. fat protein etc.) —as well as dietary diversity indices were determined using nutrition analysis software based on Austrian food composition databases [72]. A complete overview of dietary intake data is available in **Supp. Tab. 01**.

Microbial sample pre-processing - collection, DNA, RNA extraction

Participants were asked to collect oral and stool samples. Two stool samples were obtained from the same sample material. One was collected for anaerobic cultivation with eSwabs™ (Copan, USA), while the other was used for microbiome profiling (shotgun metagenomics) and placed in a sterile stool sample container (Sarstedt, Austria), which was filled with ethanol (DNA/RNA free) to preserve the sample [25]. Participants were instructed to return the samples within 24 hours of collection, keeping them at 4°C. Upon delivery, the samples for anaerobic cultivation were processed as described previously [25] before being stored alongside the samples for DNA/RNA extraction and metabolomics analysis at -80°C for future use.

DNA extraction of the original stool and oral samples was performed using the PureLink™ Microbiome DNA Purification Kit (Invitrogen, Thermo-Fisher, USA), and RNA extraction (stool) was performed using the RNeasy PowerMicrobiome Kit (Qiagen Group, Germany), following the manufacturer's instructions. Extracted DNA and RNA were stored at -80°C until further use.

Shotgun metagenomics - sequencing, data preprocessing (stool samples)

Extracted DNA of the stool samples was sequenced using the NovaSeq 6000 platform (Illumina, Eindhoven, the Netherlands) in a 2x150bp configuration at Macrogen, Seoul, South Korea. Libraries were constructed by the company using the TruSeq PCR-Free kit (350bp insert). Fastq files were received as final output after sequencing. The snakemake workflow *metagenome-atlas* (version 2.16.2) was used for quality control (QC), to filter the sequences and remove human reads (human genome: chm13v2.0) [73].

Shotgun metagenomics - taxonomic profiling (stool samples)

For taxonomic analysis, the QC sequences were taxonomically classified using *Kraken2* (version 2.1.2) with confidence setting 0.1 to retain archaeal sequences and *Bracken* (Bayesian Reestimation of Abundance with KrakEN; v2.7, read length 100) for abundance estimation [74,75]. The UHGG database (version 2.0.2) was used for both tools [76]. Subsequently, hierarchical lineage information was incorporated into the sample files using the "kreport2mpa.py" script, which is publicly available on GitHub (https://github.com/jenniferlu717/KrakenTools/blob/master/kreport2mpa.py) and feature tables of all samples were merged (**Supp. Data 01**). The reads in the final feature table were

normalized using SRS with a minimum sampling depth of 7,252,728 reads (**Supp. Data 02**) [77,78] https://github.com/CME-lab-research/AGAD/ .

Classification of Methanobrevibacter-dominant states

Methanobrevibacter-dominant states were defined based on the relative abundance of three dominant *Methanobrevibacter* taxa - *M. smithii*, *M. intestini*, and *M.* sp900766745 - in the shotgun metagenomic data derived from stool. Samples in which the overall normalized archaeal reads accounted for <0.01% of the total microbial reads were classified as having no detectable archaeal signal ("*No*" - 19/66 samples). Among samples with an archaeal signal ≥0.01%, samples were classified according to the dominating *Methanobrevibacter* taxon of the combined relative abundance of the three taxa: *M. smithii*-dominant (*Ms* - 24/66), *M. intestini*-dominant (*Mi* - 7/66), or *M.* sp900766745-dominant (*Msp* - 16/66) (**Supp. Tab. 01**).

Shotgun metagenomics - Metagenome-assembled genomes (MAGs)

Two approaches were used to retrieve metagenome-assembled genomes (MAGs). In the first approach, the focus was on the microbiome data. The previously mentioned snakemake workflow *metagenome-atlas* [73] was used to perform metagenome assembly (megahit - version1.2.9), genomic binning (MetaBAT2 - v2.15; MaxBin - v2.2.7 [79]), refining bins (DASTool - v1.1.6 [80]), dereplication (dRep - v 3.5.0 [43]), estimation of quality (CheckM2 - v 1.0.1 [81]) and taxonomic classification (GTDBtk - v2.3.2 [82,83]). The second one focused only on *Methanobrevibacter* reads and was performed using bowtie2 (v2.4.4) [84] to map shotgun reads to *M. smithii* and *M. intestini*, MAGs of our study and a UHGG reference genome of *M.* sp900766745 (UHGG database - v2.0.2: MGYG000000522/Msp900_GCA_902463315) (https://github.com/CME-lab-research/AGAD/). Subsequently, the *Methanobrevibacter*-related reads were binned (MetaBAT2 - v2.17 [79]), classified (GTBtk - v2.4.0 [82,83]), dereplicated (dRep - v 3.5.0), and quality-checked (CheckM2 – v 1.0.2 [81]) using the Nextflow (v24.04) [85] binning workflow, which can be found here: https://github.com/dienerlab/pipelines/tree/main/metagenomics.

All tools were used with default settings unless otherwise specified. Information on the MAGs can be found in **Supp. Data 03a+03b** and sequences were uploaded to the MaGe (Magnifying Genomes): Methanobrevibacter smithii MAG297, Methanobrevibacter smithii P66.1, Methanobrevibacter intestini P46.1.

The average nucleotide identity (ANI) among the three representative *Methanobrevibacter* genomes obtained from GTDB was calculated using dRep [43].

Metagenomics - analyzing the Methanobrevibacter-related functional capability

To assess the functional capability of the three *Methanobrevibacter* species, the genes of the two MAGs (*M. smithii* - MAG297; *M. intestini* - Mintestini_P46.1) as well as of one representative genome of M. sp900766745 (UHGG database - v2.0.2: MGYG000000522/Msp900_GCA_902463315) were predicted using *prodigal* [86] (v2.6.3) and functionally annotated using *eggNOG-mapper* (v2.1.8) (**Supp. Data 04a-04c**) (https://github.com/CME-lab-research/AGAD/) [87,88].

Metatranscriptomics - sequencing, data preprocessing

The sequencing library (NEBnext Ultra II (Directional) RNA Library Prep Kit) was prepared at the Core Facility for Molecular Biology at the Center for Medical Research in Graz, Austria. The sequencing was performed using the NovaSeq 6000 platform (Illumina, Eindhoven, the Netherlands) with an S2 flowcell in a 2x100bp configuration at the Vienna BioCenter Core Facilities (VBCF), Austria.

The snakemake workflow *metagenome-atlas* (version 2.16.2) was used to quality filter, assemble and functionally annotate the data as described above [73]. The final tables containing the functional information were normalized to copies per million (cpm) using the script provided by the developers: metagenome-atlas/Analyze_genecatalog.Rmd. Normalized data (cpm) was used for further analysis (**Supp. Data 05**) (https://github.com/CME-lab-research/AGAD/).

Downstream analysis and visualization

Feature tables of sequencing data (**Supp. Data 01-05**) were used for downstream taxonomic analyses. Alpha diversity metrics (Shannon, richness, evenness; **Supp. Table 10**) were calculated from SRS-normalized data, while beta diversity (bray-curtis) was assessed on rarefied data. All analyses were performed in RStudio (R version 4.3.1) [89,90]. Differential abundance analyses between predefined groups were conducted on non-normalized data using MaAsLin2 [91] and regression analysis was performed in R studio. Unless otherwise specified, all figures were generated using RStudio.

Network analyses were carried out using SCNIC (Sparse Co-occurrence Network Investigation for Compositional data) and visualized in Cytoscape (version 3.10.1; SCyNet

layout; [92]). The web-based tools NAMCO microbiome explorer and RAWGraphs (https://www.rawgraphs.io/) were used to generate bar charts, PCoA plots, and circle packing plots and sunburst diagrams, respectively [93,94].

The legends and color-blind friendly colors of the charts and graphs were adjusted using Inkscape [95]. For more details on all scripts and commands used in this manuscript, see (https://github.com/CME-lab-research/AGAD/).

Statistics on collected data

Statistical tests for different analyses, including alpha diversity indices and correlations, were performed in IBM SPSS Statistics 29 [96] or RStudio [89,90], unless stated otherwise. Based on the results of the Shapiro-Wilk test, either parametric or non-parametric tests were selected to compute p-values. To account for multiple comparisons, q-values were calculated by adjusting the p-values with Bonferroni correction for all analyses except for MaAsLin2 for which Benjamini-Hochberg correction was used.

Transporter prediction and genome-scale metabolic modelling

Metabolic models were reconstructed from ten representative genomes each of *Methanobrevibacter smithii*, *M. intestini* and *M.* sp900766745, prioritizing isolate genomes where available and complemented by high-quality MAGs (0% contamination; mean completeness 99.5%; **Supp. Tab. 06a**). Analyses were performed using gapseq v2.1.0 [97,98] within a Nextflow workflow (https://github.com/dienerlab/gapseq-docker). Reaction and pathway predictions were performed using `gapseq find` with DIAMOND v2.1.11 [99] as the sequence aligner and archaeal-specific settings (-t Archaea), followed by transporter prediction using `gapseq find-transport`. A bitscore threshold of 100 was applied for high-confidence reaction (**Supp. Tab. 06e**) and transporter predictions (**Supp. Tab. 06b**), while a lower score threshold of 50 was used during draft model construction and gap filling. Draft models were generated using `gapseq draft` and subsequently gap-filled to support a minimum growth rate of 0.01 h^{-1} (**Supp. Tab. 06h, i**). Molecular oxygen (cpd00007) was constrained to zero during medium generation, thereby enforcing anaerobic growth conditions.

For conservative comparative analyses, transporter and reaction predictions were additionally filtered using a threshold of 200 bitscore and 75% query coverage (**Supp. Tab. 06c, f**).

Resulting presence/absence matrices were used for comparative analyses (**Supp. Tab. 06d, g**). Transporters were classified according to their predicted substrates. Reaction presence, fluxes and predicted growth rates were obtained directly from the gapseq output (**Supp. Tab. 06a–i**). For selected functions, including polyphosphate kinase and exopolyphosphatase, predictions were additionally assessed using relaxed annotation thresholds to evaluate the robustness of lineage-specific differences.

Metabolomics - metabolic quantification

Nuclear magnetic resonance spectroscopy (NMR) analysis was performed at the Gottfried Schatz Research Center for Cell Signaling, Metabolism and Aging, Molecular Biology and Biochemistry, Medical University of Graz as described previously [4].

Spectra pre-processing and data analysis have been carried out using the state-of-the-art data analysis pipeline (group of Prof. Jeremy Nicholson at Imperials College London) using Matlab® scripts and MetaboAnalyst 4.0 [100]. NMR data were imported to Matlab® vR2014a (Mathworks, Natick, Massachusetts, USA), regions around the water, TSP, and remaining methanol signals excluded, and to correct for sample metabolite dilution probabilistic quotient normalization [101] was performed. **Supp. Data 06** lists all metabolites quantified as arbitrary units revealed by peak integration, which are proportional to concentrations.

Cultivation - tracer experiment

One isolate of *M. smithii* (P31) and *M. intestini* (P45), respectively, were cultivated in MS medium in triplicates. Enrichment and isolation of the *Methanobrevibacter* species was described elsewhere [25]. At the time of inoculation sodium acetate was replaced by 10 mM $^{13}C_2$ acetate. One culture of each *Methanobrevibacter* strain was treated as control (without tracer). Cells were harvested after 26 h by centrifugation at 8000 rpm for 2 mins. Supernatant was transferred into fresh 1.5 mL tubes and pellets were washed in 1 ml 0.9% NaCl. The supernatant and pellets were shock-frozen and stored at -80°C until further use.
Cell pellets were extracted in chilled 62.5% methanol containing norvaline as an internal standard. After brief sonication in a water bath, chloroform was added for biphasic extraction. Samples were vortexed, centrifuged and the polar (aqueous) phase was transferred and dried down in a vacuum centrifuge. For derivatisation, samples were reconstituted in 20 µL methoxyamine (MOX) reagent (Thermo Fisher Scientific, USA) and incubated at 37°C for 60 minutes, followed by 30 µL *N*-tert-butyldimethylsilyl-*N*-methyltrifluoroacetamide with 1% tert-

butyldimethylchlorosilane (MTBSTFA + 1% TBDMS, Thermo Fisher Scientific) and an incubation for 30 minutes at 60°C. Derivatized samples were analyzed by gas chromatography-mass spectrometry (GC-MS) analysis on an Agilent 7890B GC coupled to a 5977A Inert MSD system (Agilent Technologies, USA). A DB-35 ms column and helium as carrier gas with a flow rate of 1 mL/min was used for chromatographic separation. The injection volume was 1 µL and measurements were taken in splitless mode with an inlet temperature of 270°C; the oven program held 100°C for 3 minutes and ramped to 300°C at 3.5°C/min. Mass spectra were acquired in electron-ionization (EI) mode at 70 eV across m/z 100-605. Peak integration and isotopologue analysis were carried out in EI-Maven [102] and natural abundance correction was performed with IsoCor [103].

References

1. Chibani, C. M. *et al.* A catalogue of 1,167 genomes from the human gut archaeome. *Nat. Microbiol.* **7**, 48–61 (2022).
2. Hoegenauer, C., Hammer, H. F., Mahnert, A. & Moissl-Eichinger, C. Methanogenic archaea in the human gastrointestinal tract. *Nat. Rev. Gastroenterol. Hepatol.* **19**, 805–813 (2022).
3. Ruaud, A. *et al.* Syntrophy via interspecies H2 transfer between christensenella and methanobrevibacter underlies their global cooccurrence in the human gut. *mBio* **11**, (2020).
4. Kumpitsch, C. *et al.* Reduced B12 uptake and increased gastrointestinal formate are associated with archaeome-mediated breath methane emission in humans. *Microbiome* **9**, (2021).
5. Polag, D. & Keppler, F. Global methane emissions from the human body: Past, present and future. *Atmos. Environ.* **214**, 116823 (2019).
6. Polag, D., Leiß, O. & Keppler, F. Age dependent breath methane in the German population. *Science of The Total Environment* **481**, 582–587 (2014).
7. Mehravar, S. *et al.* Symptom Profile of Patients With Intestinal Methanogen Overgrowth: A Systematic Review and Meta-analysis. *Clinical Gastroenterology and Hepatology* **23**, 1111-1122.e9 (2025).
8. Kim, G. *et al.* Methanobrevibacter smithii Is the Predominant Methanogen in Patients with Constipation-Predominant IBS and Methane on Breath. *Dig Dis Sci* **57**, 3213–3218 (2012).
9. Mohammadzadeh, R. *et al.* Age-related dynamics of predominant methanogenic archaea in the human gut microbiome. *BMC Microbiology 2025 25:1* **25**, 193- (2025).
10. Mohammadzadeh, R. *et al. Methanobrevibacter smithii* associates with colorectal cancer through trophic control of the cancer bacteriome. https://doi.org/10.1101/2025.06.12.659283 (2025) doi:10.1101/2025.06.12.659283.
11. Sirimongkolkasem, J. *et al.* Methane Trajectory Phenotypes on Glucose Breath Testing Are Associated With Slow Colonic Transit: A Group-Based Trajectory Modeling Analysis. *Neurogastroenterology and Motility* **38**, e70409 (2026).
12. Holma, R. *et al.* Colonic methanogenesis in vivo and in vitro and fecal pH after resection of colorectal cancer and in healthy intact colon. *International Journal of Colorectal Disease 2011 27:2* **27**, 171–178 (2011).
13. Dirks, B. *et al.* Methanogenesis associated with altered microbial production of short-chain fatty acids and human-host metabolizable energy. *ISME J.* **19**, 103 (2025).
14. Campbell, A., Gdanetz, K., Schmidt, A. W. & Schmidt, T. M. H2 generated by fermentation in the human gut microbiome influences metabolism and competitive fitness of gut butyrate producers. *Microbiome 2023 11:1* **11**, 133- (2023).
15. Carbonero, F., Benefiel, A. C. & Gaskins, H. R. Contributions of the microbial hydrogen economy to colonic homeostasis. *Nat. Rev. Gastroenterol. Hepatol.* **9**, 504–518 (2012).
16. Samuel, B. S. *et al.* Genomic and metabolic adaptations of Methanobrevibacter smithii to the human gut. *Proc. Natl. Acad. Sci. U. S. A.* **104**, 10643–10648 (2007).
17. Baker, B. J. *et al.* Diversity, ecology and evolution of Archaea. *Nature Microbiology 2020 5:7* **5**, 887–900 (2020).
18. Mahnert, A., Blohs, M., Pausan, M. R. & Moissl-Eichinger, C. The human archaeome: Methodological pitfalls and knowledge gaps. *Emerg. Top. Life Sci.* **2**, 469–482 (2018).
19. Youngblut, N. D. *et al.* Vertebrate host phylogeny influences gut archaeal diversity. *Nat. Microbiol.* **6**, 1443–1454 (2021).
20. Protasov, E. *et al.* Taxonomic revision of the genus Methanobrevibacter, description of Methanomonile shimae gen. nov. sp. nov., and proposal of Methanobrevibacteraceae fam. nov. *Int. J. Syst. Evol. Microbiol.* **76**, 007286 (2026).
21. Hansen, E. E. *et al.* Pan-genome of the dominant human gut-associated archaeon, Methanobrevibacter smithii, studied in twins. *Proc. Natl. Acad. Sci. U. S. A.* **108**, 4599–4606 (2011).

22. Pasolli, E. *et al.* Extensive Unexplored Human Microbiome Diversity Revealed by Over 150,000 Genomes from Metagenomes Spanning Age, Geography, and Lifestyle. *Cell* **176**, (2019).
23. Weinberger, V. *et al.* Expanding the cultivable human archaeome: Methanobrevibacter intestini sp. nov. and strain Methanobrevibacter smithii 'GRAZ-2' from human faeces. *Int. J. Syst. Evol. Microbiol.* **75**, (2025).
24. Candeliere, F., Sola, L., Raimondi, S., Rossi, M. & Amaretti, A. Good and bad dispositions between archaea and bacteria in the human gut: New insights from metagenomic survey and co-occurrence analysis. *Synth. Syst. Biotechnol.* **9**, 88–98 (2024).
25. Duller, S. *et al.* Targeted isolation of Methanobrevibacter strains from fecal samples expands the cultivated human archaeome. *Nature Communications* **15**, (2024).
26. Sun, X. W. *et al.* Christensenella strain resources, genomic/metabolomic profiling, and association with host at species level. *Gut Microbes* **16**, (2024).
27. Gophna, U., Konikoff, T. & Nielsen, H. B. Oscillospira and related bacteria – From metagenomic species to metabolic features. *Environ. Microbiol.* **19**, 835–841 (2017).
28. Procházková, N. *et al.* Gut physiology and environment explain variations in human gut microbiome composition and metabolism. *Nature Microbiology 2024 9:12* **9**, 3210–3225 (2024).
29. Hillman, E. B. M. *et al.* Changing Gastrointestinal Transit Time Alters Microbiome Composition and Bile Acid Metabolism: A Cross-Over Study in Healthy Volunteers. *Neurogastroenterology and Motility* **37**, e70075 (2025).
30. Roager, H. M. *et al.* Colonic transit time is related to bacterial metabolism and mucosal turnover in the gut. *Nature Microbiology 2016 1:9* **1**, 16093- (2016).
31. Zheng, D., Liwinski, T. & Elinav, E. Interaction between microbiota and immunity in health and disease. *Cell Research 2020 30:6* **30**, 492–506 (2020).
32. Jalandra, R., Makharia, G. K., Sharma, M. & Kumar, A. Inflammatory and deleterious role of gut microbiota-derived trimethylamine on colon cells. *Front. Immunol.* **13**, 1101429 (2023).
33. Ramezani, A. *et al.* Gut Colonization with Methanogenic Archaea Lowers Plasma Trimethylamine N-oxide Concentrations in Apolipoprotein e−/− Mice. *Scientific Reports 2018 8:1* **8**, 14752- (2018).
34. Fu, B. C. *et al.* Associations of plasma trimethylamine N-oxide, choline, carnitine, and betaine with inflammatory and cardiometabolic risk biomarkers and the fecal microbiome in the Multiethnic Cohort Adiposity Phenotype Study. *Am. J. Clin. Nutr.* **111**, 1226–1234 (2020).
35. Wang, Z. *et al.* Gut flora metabolism of phosphatidylcholine promotes cardiovascular disease. *Nature 2011 472:7341* **472**, 57–63 (2011).
36. Janeiro, M. H., Ramírez, M. J., Milagro, F. I., Martínez, J. A. & Solas, M. Implication of Trimethylamine N-Oxide (TMAO) in Disease: Potential Biomarker or New Therapeutic Target. *Nutrients 2018, Vol. 10, Page 1398* **10**, 1398 (2018).
37. Braga, J. D., Thongngam, M. & Kumrungsee, T. Gamma-aminobutyric acid as a potential postbiotic mediator in the gut–brain axis. *npj Science of Food 2024 8:1* **8**, 16- (2024).
38. Richard, H. & Foster, J. W. Escherichia coli glutamate- and arginine-dependent acid resistance systems increase internal pH and reverse transmembrane potential. *J. Bacteriol.* **186**, 6032–6041 (2004).
39. Feehily, C. & Karatzas, K. A. G. Role of glutamate metabolism in bacterial responses towards acid and other stresses. *J. Appl. Microbiol.* **114**, 11–24 (2013).
40. van Deuren, T. *et al.* Specific dietary fibers steer toward distal colonic saccharolytic fermentation using the microbiota of individuals with overweight/obesity. *Food Research International* **209**, (2025).
41. Leite, G. G. S. *et al.* Mapping the Segmental Microbiomes in the Human Small Bowel in Comparison with Stool: A REIMAGINE Study. *Digestive Diseases and Sciences 2020 65:9* **65**, 2595–2604 (2020).
42. Levitan, O. *et al.* The gut microbiome–Does stool represent right? *Heliyon* **9**, (2023).

43. Olm, M. R., Brown, C. T., Brooks, B. & Banfield, J. F. DRep: A tool for fast and accurate genomic comparisons that enables improved genome recovery from metagenomes through de-replication. *ISME Journal* **11**, 2864–2868 (2017).
44. Pimentel, M. *et al.* Methane, a gas produced by enteric bacteria, slows intestinal transit and augments small intestinal contractile activity. *Am. J. Physiol. Gastrointest. Liver Physiol.* **290**, (2006).
45. Jahng, J., Jung, I. S., Choi, E. J., Conklin, J. L. & Park, H. The effects of methane and hydrogen gases produced by enteric bacteria on ileal motility and colonic transit time. *Neurogastroenterology and Motility* **24**, (2012).
46. Park, Y. M., Lee, Y. J., Hussain, Z., Lee, Y. H. & Park, H. The effects and mechanism of action of methane on ileal motor function. *Neurogastroenterology and Motility* **29**, e13077 (2017).
47. Villanueva-Millan, M. J. *et al.* Methanogens and Hydrogen Sulfide Producing Bacteria Guide Distinct Gut Microbe Profiles and Irritable Bowel Syndrome Subtypes. *Am. J. Gastroenterol.* **117**, 2055–2066 (2022).
48. Minnebo, Y. *et al.* Gut microbiota response to in vitro transit time variation is mediated by microbial growth rates, nutrient use efficiency and adaptation to in vivo transit time. *Microbiome 2023 11:1* **11**, 240- (2023).
49. Koh, A., De Vadder, F., Kovatcheva-Datchary, P. & Bäckhed, F. From dietary fiber to host physiology: Short-chain fatty acids as key bacterial metabolites. *Cell* **165**, 1332–1345 (2016).
50. Smith, E. A. & Macfarlane, G. T. Dissimilatory Amino Acid Metabolism in Human Colonic Bacteria. *Anaerobe* **3**, 327–337 (1997).
51. Procházková, N. *et al.* Advancing human gut microbiota research by considering gut transit time. *Gut* **72**, 180–191 (2023).
52. Conlon, M. A. & Bird, A. R. The Impact of Diet and Lifestyle on Gut Microbiota and Human Health. *Nutrients 2015, Vol. 7, Pages 17-44* **7**, 17–44 (2014).
53. Macfarlane, G. T., Gibson, G. R. & Cummings, J. H. Comparison of fermentation reactions in different regions of the human colon. *Journal of Applied Bacteriology* **72**, 57–64 (1992).
54. Walker, A. W., Duncan, S. H., Carol McWilliam Leitch, E., Child, M. W. & Flint, H. J. pH and Peptide Supply Can Radically Alter Bacterial Populations and Short-Chain Fatty Acid Ratios within Microbial Communities from the Human Colon. *Appl. Environ. Microbiol.* **71**, 3692–3700 (2005).
55. Waters, J. L. & Ley, R. E. The human gut bacteria Christensenellaceae are widespread, heritable, and associated with health. *BMC Biology 2019 17:1* **17**, 83- (2019).
56. Näpflin, N., Schubert, C., Malfertheiner, L., Hardt, W. D. & von Mering, C. Gene-level analysis of core carbohydrate metabolism across the Enterobacteriaceae pan-genome. *Communications Biology 2025 8:1* **8**, 1241- (2025).
57. Boets, E. *et al.* Systemic availability and metabolism of colonic-derived short-chain fatty acids in healthy subjects: a stable isotope study. *Journal of Physiology* **595**, 541–555 (2017).
58. Smith, N. W., Shorten, P. R., Altermann, E. H., Roy, N. C. & McNabb, W. C. Hydrogen cross-feeders of the human gastrointestinal tract. *Gut Microbes* **10**, 270–288 (2019).
59. Nava, G. M., Carbonero, F., Croix, J. A., Greenberg, E. & Gaskins, H. R. Abundance and diversity of mucosa-associated hydrogenotrophic microbes in the healthy human colon. *The ISME Journal 2012 6:1* **6**, 57–70 (2011).
60. Amaretti, A. *et al.* Profiling of Protein Degraders in Cultures of Human Gut Microbiota. *Front. Microbiol.* **10**, 2614 (2019).
61. Andriamihaja, M. *et al.* The deleterious metabolic and genotoxic effects of the bacterial metabolite p-cresol on colonic epithelial cells. *Free Radic. Biol. Med.* **85**, 219–227 (2015).
62. Pedersen, G., Brynskov, J. & Saermark, T. Phenol Toxicity and Conjugation in Human Colonic Epithelial Cells. *Scand. J. Gastroenterol.* **37**, 74–79 (2002).
63. Gilbert, M. S., Ijssennagger, N., Kies, A. K. & van Mil, S. W. C. Protein fermentation in the gut; implications for intestinal dysfunction in humans, pigs, and poultry. *https://doi.org/10.1152/ajpgi.00319.2017* **315**, G159–G170 (2018).

64. Gibson, G. R., MacFarlane, G. T. & Cummings, J. H. Sulphate reducing bacteria and hydrogen metabolism in the human large intestine. *Gut* **34**, 437–439 (1993).
65. Bernalier, A. *et al.* Acetogenesis from H2 and CO2 by methane- and non-methane-producing human colonic bacterial communities. *FEMS Microbiol. Ecol.* **19**, 193–202 (1996).
66. Thauer, R. K., Jungermann, K. & Decker, K. Energy conservation in chemotrophic anaerobic bacteria. *Bacteriol. Rev.* **41**, 100–180 (1977).
67. Gibson, G. R., Macfarlane, G. T. & Cummings, J. H. Occurrence of sulphate-reducing bacteria in human faeces and the relationship of dissimilatory sulphate reduction to methanogenesis in the large gut. *Journal of Applied Bacteriology* **65**, 103–111 (1988).
68. Thwaites, P. A. *et al.* Telemetric Assessment and Comparison of Regional Colonic Metabolic Activity in Ambulant Healthy Individuals Using pH and Gas-Sensing Wireless Motility Capsules. *Aliment. Pharmacol. Ther.* **63**, 242 (2025).
69. Martins, M. & Pereira, I. A. C. Sulfate-reducing bacteria as new microorganisms for biological hydrogen production. *Int. J. Hydrogen Energy* **38**, 12294–12301 (2013).
70. Martins, M., Mourato, C. & Pereira, I. A. C. Desulfovibrio vulgaris Growth Coupled to Formate-Driven H2 Production. *Environ. Sci. Technol.* **49**, 14655–14662 (2015).
71. Haftenberger, M. *et al.* Relative validation of a food frequency questionnaire for national health and nutrition monitoring. *Nutr. J.* **9**, (2010).
72. dato Denkwerkzeuge. nut.s science (v1.33.25) [Software]. Preprint at www.nutritional-software.at (2024).
73. Kieser, S., Brown, J., Zdobnov, E. M., Trajkovski, M. & McCue, L. A. ATLAS: a Snakemake workflow for assembly, annotation, and genomic binning of metagenome sequence data. *BMC Bioinformatics 2020 21:1* **21**, 257- (2020).
74. Wood, D. E., Lu, J. & Langmead, B. Improved metagenomic analysis with Kraken 2. *Genome Biology 2019 20:1* **20**, 257- (2019).
75. Lu, J., Breitwieser, F. P., Thielen, P. & Salzberg, S. L. Bracken: Estimating species abundance in metagenomics data. *PeerJ Comput. Sci.* **2017**, e104 (2017).
76. Almeida, A. *et al.* A unified catalog of 204,938 reference genomes from the human gut microbiome. *Nat. Biotechnol.* **39**, 105–114 (2021).
77. Heidrich, V., Karlovsky, P. & Beule, L. 'SRS' R Package and 'q2-srs' QIIME 2 Plugin: Normalization of Microbiome Data Using Scaling with Ranked Subsampling (SRS). *Applied Sciences* **11**, 11473 (2021).
78. Beule, L. & Karlovsky, P. Improved normalization of species count data in ecology by scaling with ranked subsampling (SRS): application to microbial communities. *PeerJ* **8**, e9593 (2020).
79. Kang, D. D. *et al.* MetaBAT 2: An adaptive binning algorithm for robust and efficient genome reconstruction from metagenome assemblies. *PeerJ* **2019**, e7359 (2019).
80. Sieber, C. M. K. *et al.* Recovery of genomes from metagenomes via a dereplication, aggregation and scoring strategy. *Nature Microbiology 2018 3:7* **3**, 836–843 (2018).
81. Chklovski, A., Parks, D. H., Woodcroft, B. J. & Tyson, G. W. CheckM2: a rapid, scalable and accurate tool for assessing microbial genome quality using machine learning. *Nature Methods 2023 20:8* **20**, 1203–1212 (2023).
82. Chaumeil, P. A., Mussig, A. J., Hugenholtz, P. & Parks, D. H. GTDB-Tk: A toolkit to classify genomes with the genome taxonomy database. *Bioinformatics* **36**, 1925–1927 (2020).
83. Parks, D. H. *et al.* GTDB: an ongoing census of bacterial and archaeal diversity through a phylogenetically consistent, rank normalized and complete genome-based taxonomy. *Nucleic Acids Res.* **50**, D785–D794 (2022).
84. Langmead, B. & Salzberg, S. L. Fast gapped-read alignment with Bowtie 2. *Nat. Methods* **9**, 357–359 (2012).
85. DI Tommaso, P. *et al.* Nextflow enables reproducible computational workflows. *Nature Biotechnology 2017 35:4* **35**, 316–319 (2017).
86. Hyatt, D. *et al.* Prodigal: prokaryotic gene recognition and translation initiation site identification. *BMC Bioinformatics 2010 11:1* **11**, 119- (2010).

87. Cantalapiedra, C. P., Herņandez-Plaza, A., Letunic, I., Bork, P. & Huerta-Cepas, J. eggNOG-mapper v2: Functional Annotation, Orthology Assignments, and Domain Prediction at the Metagenomic Scale. *Mol. Biol. Evol.* **38**, 5825–5829 (2021).
88. Huerta-Cepas, J. *et al.* eggNOG 5.0: a hierarchical, functionally and phylogenetically annotated orthology resource based on 5090 organisms and 2502 viruses. *Nucleic Acids Res.* **47**, D309–D314 (2019).
89. RStudio Team. RStudio: Integrated Development Environment for R. Preprint at http://www.rstudio.com/ (2019).
90. R Core Team. R: A Language and Environment for Statistical Computing. Preprint at https://www.r-project.org (2020).
91. Mallick, H. *et al.* Multivariable association discovery in population-scale meta-omics studies. *PLoS Comput. Biol.* **17**, e1009442 (2021).
92. Shannon, P. *et al.* Cytoscape: A Software Environment for Integrated Models of Biomolecular Interaction Networks. *Genome Res.* **13**, 2498–2504 (2003).
93. Dietrich, A. *et al.* Namco: a microbiome explorer. *Microb. Genom.* **8**, 000852 (2022).
94. Mauri, M., Elli, T., Caviglia, G., Uboldi, G. & Azzi, M. RAWGraphs: A Visualisation Platform to Create Open Outputs. Preprint at https://doi.org/https://doi.org/10.1145/3125571.3125585 (2017).
95. Inkscape Project. Inkscape. Preprint at https://inkscape.org (2020).
96. IBM Corp. IBM SPSS Statistics for Windows. Preprint at (2019).
97. De Bernardini, N. *et al.* pan-Draft: automated reconstruction of species-representative metabolic models from multiple genomes. *Genome Biology 2024 25:1* **25**, 280- (2024).
98. Zimmermann, J., Kaleta, C. & Waschina, S. gapseq: informed prediction of bacterial metabolic pathways and reconstruction of accurate metabolic models. *Genome Biology 2021 22:1* **22**, 81- (2021).
99. Buchfink, B., Reuter, K. & Drost, H. G. Sensitive protein alignments at tree-of-life scale using DIAMOND. *Nature Methods 2021 18:4* **18**, 366–368 (2021).
100. Pang, Z. *et al.* MetaboAnalystR 4.0: a unified LC-MS workflow for global metabolomics. *Nature Communications 2024 15:1* **15**, 3675- (2024).
101. Dieterle, F., Ross, A., Schlotterbeck, G. & Senn, H. Probabilistic quotient normalization as robust method to account for dilution of complex biological mixtures. Application in1H NMR metabonomics. *Anal. Chem.* **78**, 4281–4290 (2006).
102. Agrawal, S. *et al.* EL-MAVEN: A fast, robust, and user-friendly mass spectrometry data processing engine for metabolomics. *Methods in Molecular Biology* **1978**, 301–321 (2019).
103. Millard, P. *et al.* IsoCor: isotope correction for high-resolution MS labeling experiments. *Bioinformatics* **35**, 4484–4487 (2019).

Supplementary Files

This is a list of supplementary files associated with this preprint. Click to download.

- Table1AGAD.png
- SupplementaryFiguresAGAD.docx
- SupplementaryDataAGAD.xlsx
- AGADSupplementaryTablesv01.xlsx